Supplementary Information (SI) for Dalton Transactions.

Highly Efficient Photocatalytic Reduction of CO_2 to CO under Visible Light Using Rhenium Benzo[d]Oxazole Complexes†

Uday Shee[a], Biswajit Khutia[a], Sneha Ray[a], Sumona Ghosh[a], Kajal Krishna Rajak[a*]

[a]Inorganic Chemistry Section, Department of Chemistry, Jadavpur University, Kolkata- 700032, Email id: kajalk.rajak@jadavpuruniversity.in ; kajalrajak@rediffmail.com

Electronic Supplementary Information (ESI)

Table of Contents **Page No.**

Materials: Toluene, hexane, ethyl acetate, methanol, dichloromethane, *N,N*-dimethylformamide, and triethylamine were acquired from Mark and subjected to drying prior to use. 2-Picolylamine, 3,5-di-tert-butylcatechol, 2-picolinic acid, quinoline-2-carboxylic acid hydrochloride, 1-amino-2-naphthol hydrochloride, 3-amino-2-naphthol, Isoquinoline-1-carboxylic acid, 2,2,2-trifluoroethanol, 2,3-dihydro-1,3-dimethyl-2-phenylbenzimidazole(BIH), and pentacarbonylchlororhenium(I) were purchased from Sigma-Aldrich. Electrochemical-grade tetrabutylammonium hexafluorophosphate ($[^nBu_4N]PF_6$) with a minimum purity of 99.0% was also obtained from Sigma-Aldrich.

Instrumentation Details:

X-Ray crystallography:

The X-ray intensity data were recorded on Bruker AXS SMART APEX CCD diffractometer (Mo K_α, λ = 0.71073 Å) at 293 K. A total of 606 frames were collected with a scan width of 0.3° in different settings of φ. The data were reduced in SAINTPLUS[1] and empirical absorption correction was applied using the SADABS package. Metal atom was located by Patterson method and the rest of the non-hydrogen atoms were emerged from successive Fourier synthesis. The structures were refined by full matrix least-square procedure on F^2. All non-hydrogen atoms were refined anisotropically. All the calculations were performed using the SHELXTL V 6.14 program package[2]. Molecular structure plots were drawn using the Oak Ridge thermal ellipsoid plot (Ortep)

Physical Measurements :

^{1}H NMR spectra were recorded on Bruker FT 300 MHz spectrometer, where tetramethylsilane (TMS) was used as an internal reference and DMSO-d_6 was used as solvent. Micromass Q-Tof YA 263 mass spectrometer and Bruker Maxis Q-Tof ESI-MS were used to record the Electro-spray ionization mass spectrometry (ESI-MS) of the molecules. Elemental analyses (C, H, and N) of the synthesized molecules were carried out using Perkin–Elmer 2400 series II analyser. IR spectra were measured by Perkin–Elmer L-0100 spectrophotometer. The X-ray intensity data were collected on Bruker AXS SMART APEX CCD. UV–Vis spectra were measured by using a Shimadzu UV-VIS Spectrophotometer: UV 19001. Fluorescence spectroscopic studies were performed by using Horiba Fluoromax-4 spectrofluorometer. Electrochemical measurements were accomplished with the help of CHI600E electrochemical analyser using glassy carbon electrode under nitrogen atmosphere. Tetrabutylammoniumhexafluorophosphate was used as a supporting electrolyte and potentials were referenced to the Standard Calomel Electrode without junction correction. The impedance measurements were carried out using CHI760E workstation (CHI Instruments, USA) through a conventional three-electrode system. Quantum yield of the complexes was determined in freeze-pump-thaw-degassed solutions of the complexes using quinine sulphate and fluorescein in the same solvent as the standard [Φ_{std}=0.54 at 298 K in 0.1 M H_2SO_4 at λ_{ex}=350 nm] by usual method. The quantum yields were calculated by using Eq. S1.

$$\Phi_r = \Phi_{std}\frac{A_{std}\, I_r\ \eta_r^2}{A_r\ I_{std}\eta_{std}^2} \qquad \text{Eq.S1}$$

where Φ_r and Φ_{std} are the quantum yields of unknown and standard samples, A_r and A_{std} refer to the solution absorbances at the excitation wavelength (λ_{ex}), I_r and I_{std} are the integrated emission intensities, η_r and η_{std} are the refractive indices of the solvent. Time-correlated-single-photon-counting (TCSPC) measurements were performed for the luminescence decay of the complexes in acetonitrile and dichloromethane. The fluorescence decay data were collected on a Hamamatsu MCP photomultiplier (R3809) and were analysed by using IBH DAS6 software.

Gas Detection by Gas Chromatography (GC):

The gas evolved during BE was detected by using GC instrument of model no. 8860 (G2790A), serial no. CN2211C039 fitted with TCD. 500 µl gases was syringed out by a gas tight syringe from the head space of the working chamber of the H cell and was injected into the inlet of the GC.

Computational Study:

The geometrical structures of the singlet ground state and triplet excited state of the synthesized Re complexes were optimized by the DFT method[3] using B3LYP exchange correlation functional[4] approach. The geometry of the Re complexes was fully optimized in solution phase (namely dichloromethane and acetonitrile) without any symmetry constraints. There was a good agreement between the theoretically modelled and experimental structures. Based on the optimized ground state geometry, both the absorption and emission properties in acetonitrile and dichloromethane solvent was calculated by time-dependent density functional theory (TDDFT)[5] approaches related with the conductor-like polarizable continuum model (CPCM).[6] We computed the lowest 50 singlet – singlet transition and the results obtained from the TD calculations were qualitatively very similar. The TDDFT approach had been established to be reliable for calculating spectral properties of many transition metal complexes.[7] Due to the presence of electronic correlation in the TDDFT (B3LYP) method it can yield more accurate electronic excitation energies. Hence TDDFT had been shown to provide a reasonable spectral feature for the complexes of our examination. In the calculation, the quasi-relativistic pseudo potentials of Re atoms were predicted by using Hay and Wadt[8] with 14 valence electrons [outer-core ($5s^25p^6$) electrons and the ($5d^6$) valence electrons] were employed, and a "double-ξ" quality basis set LANL2DZ was adopted as the basis set for Re atoms. For H 6-31(g) basis set was used and the 6-31+ G (d, p) basis set was used for C, N, O and Cl atoms for the optimization of the ground state and excited state geometries. Gauss View 5.1 software was utilized to originate the figures showing MOs and the difference density plots. All the calculations were performed with the Gaussian 09W software package.[9]

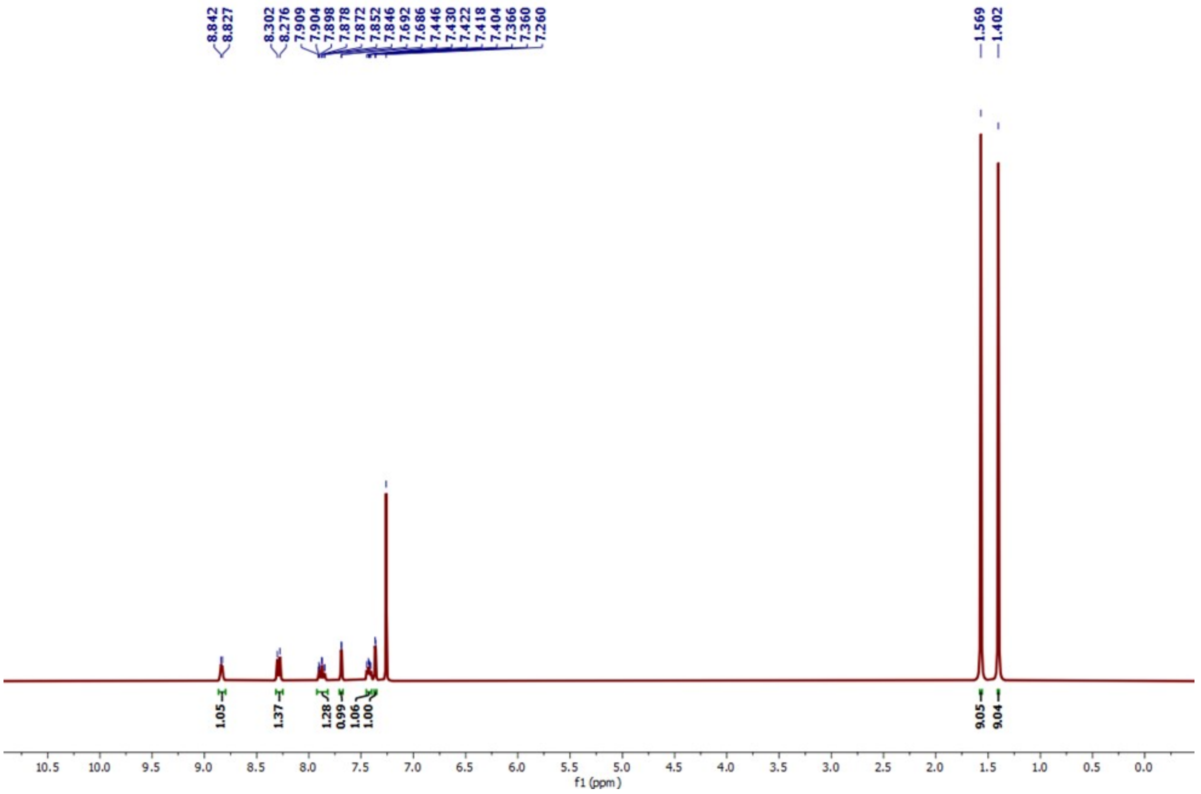

Fig. S1: ^{1}H NMR Spectrum of Ligand-1a in $CDCl_3$

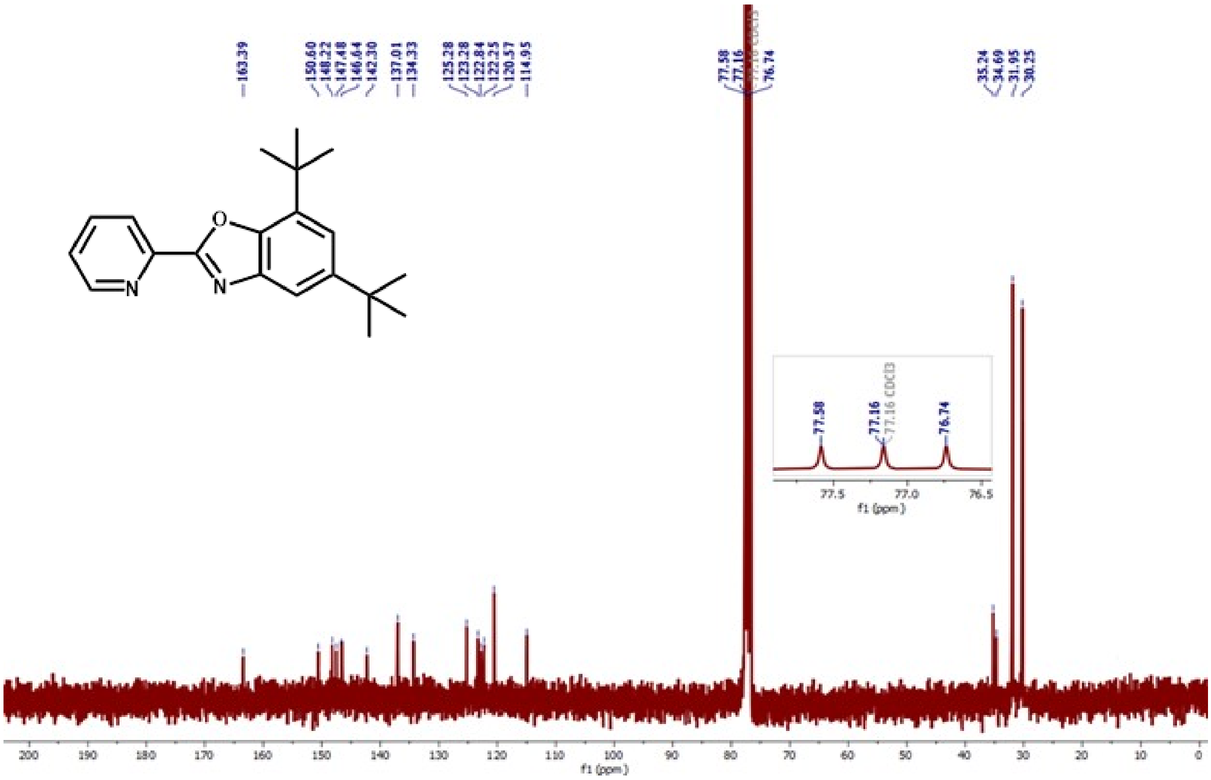

Fig. S2: ^{13}C NMR Spectrum of Ligand-1a in $CDCl_3$

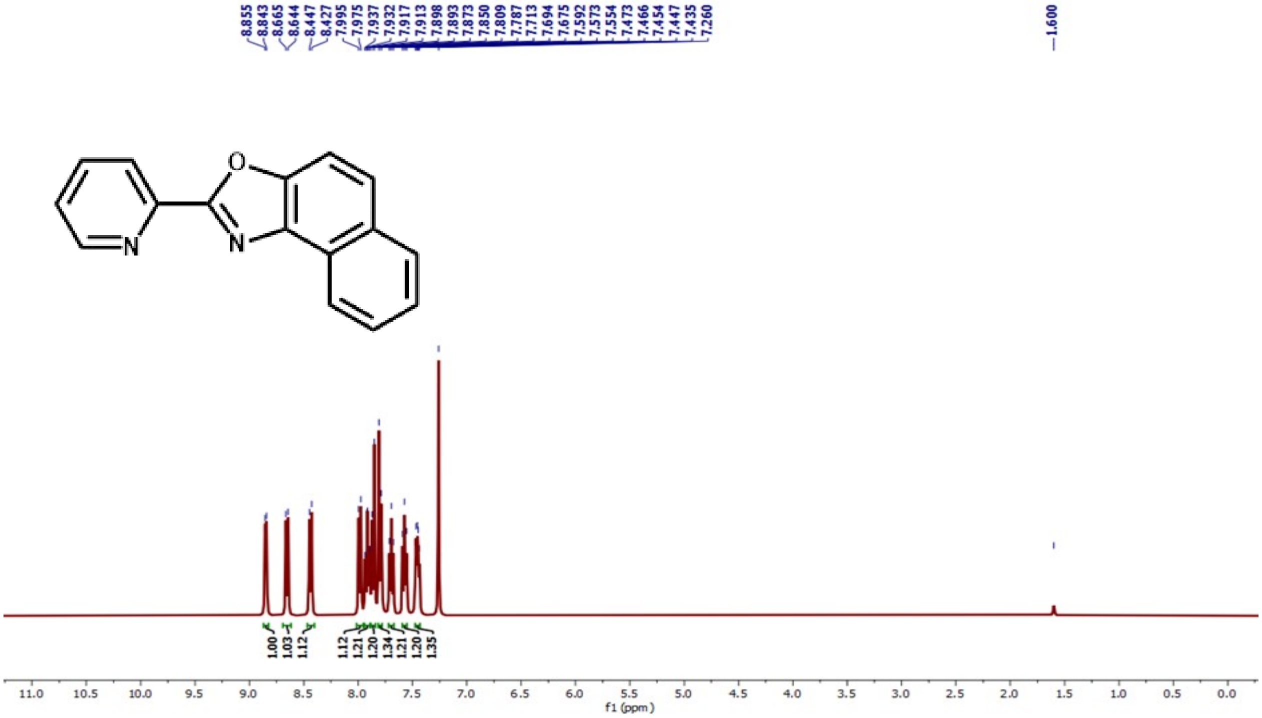

Fig. S3: ^{1}H NMR Spectrum of Ligand-1b in $CDCl_3$

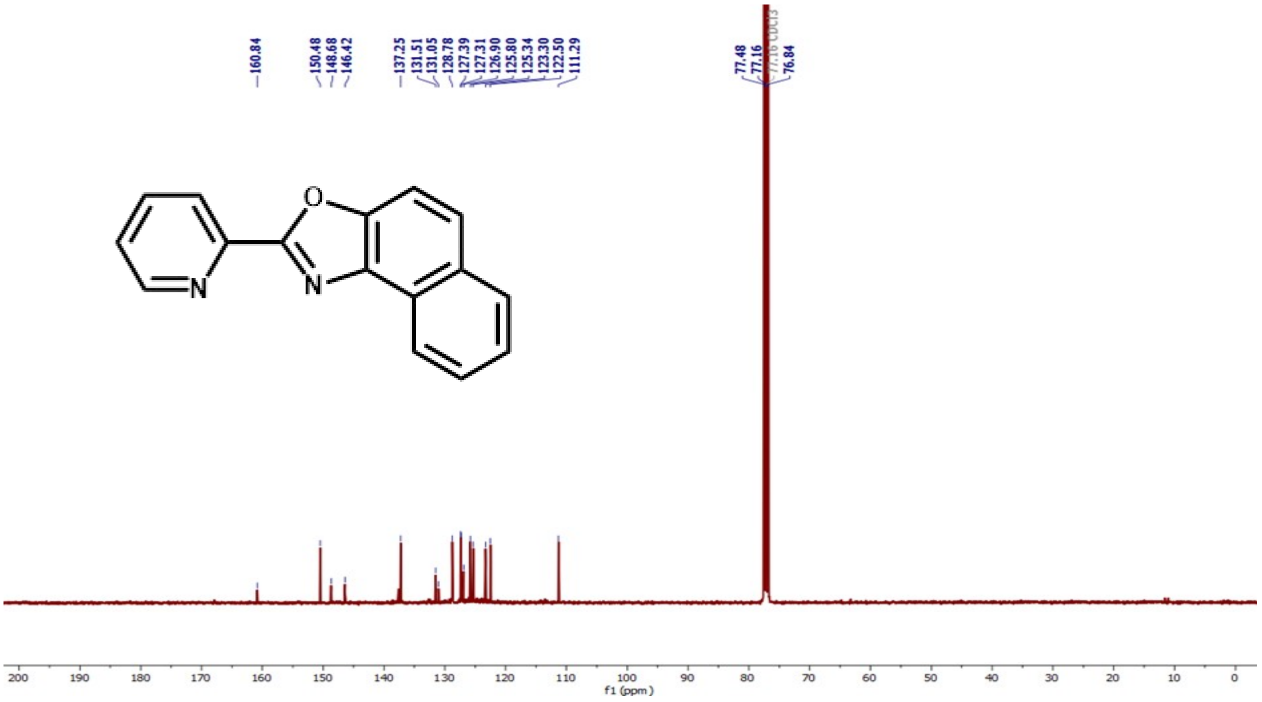

Fig. S4: ^{13}C NMR Spectrum of Ligand-1b in $CDCl_3$

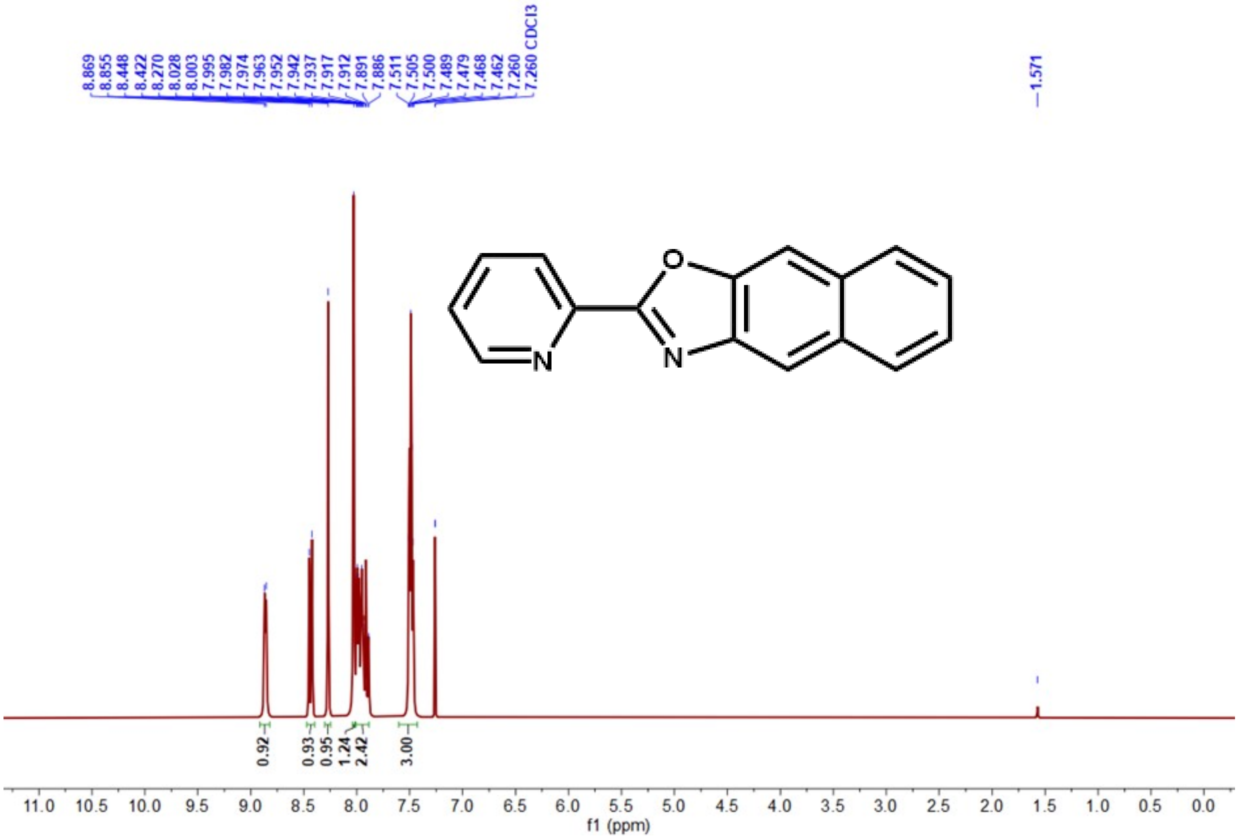

Fig. S5: ^{1}H NMR Spectrum of Ligand-1c in $CDCl_3$

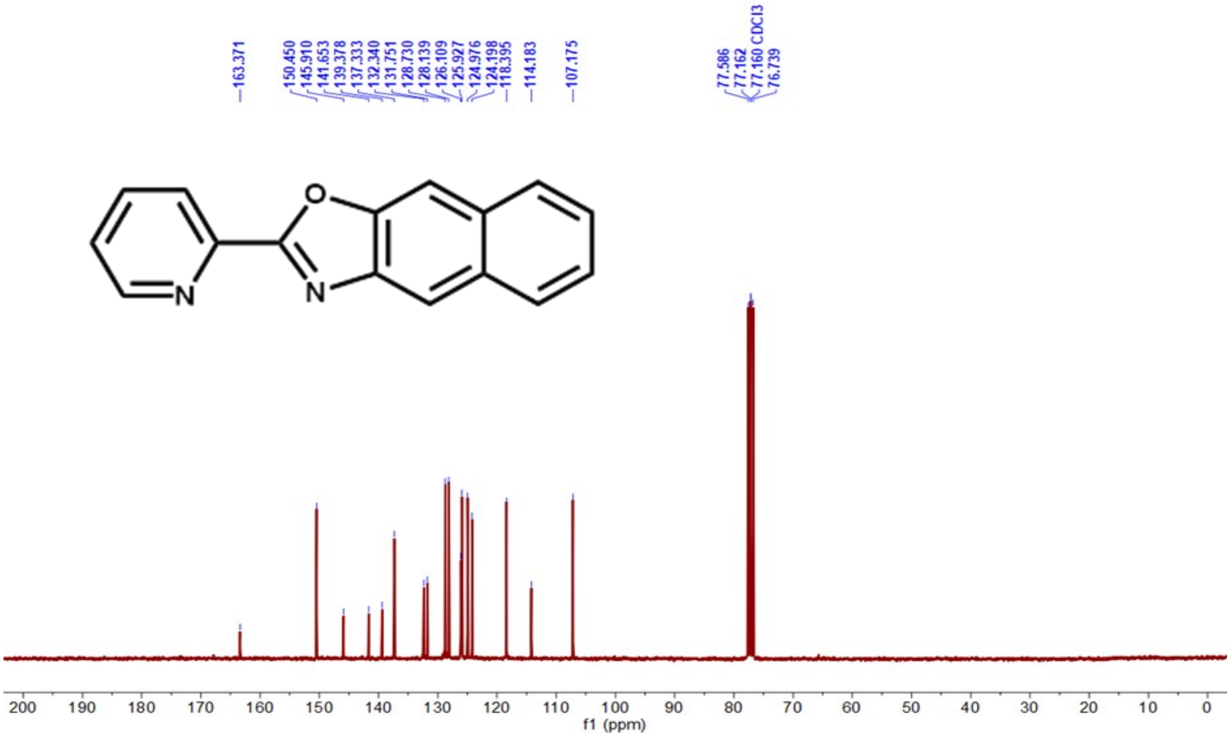

Fig. S6: ^{13}C NMR Spectrum of Ligand-1c in $CDCl_3$

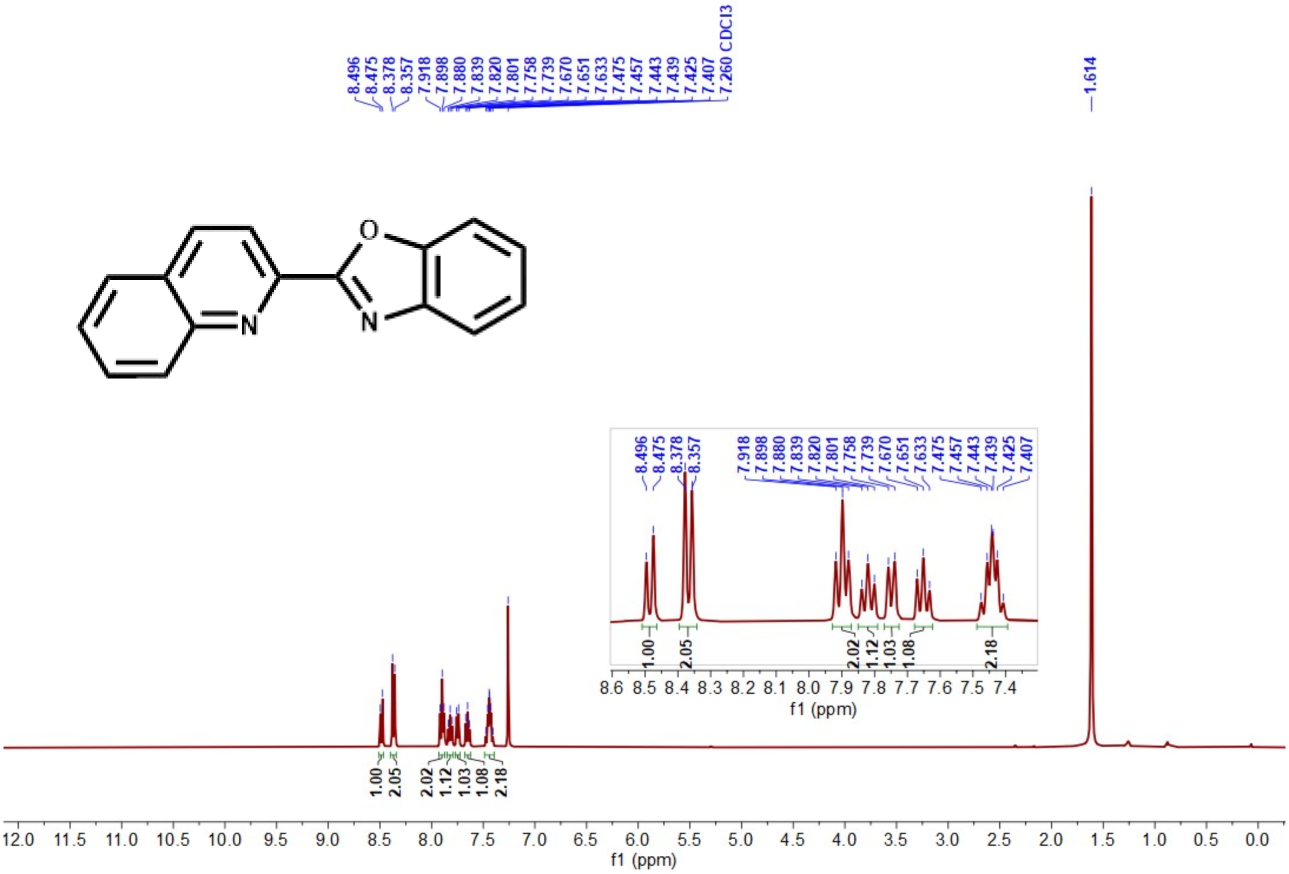

Fig. S7: ^{1}H NMR Spectrum of Ligand-2a in $CDCl_3$

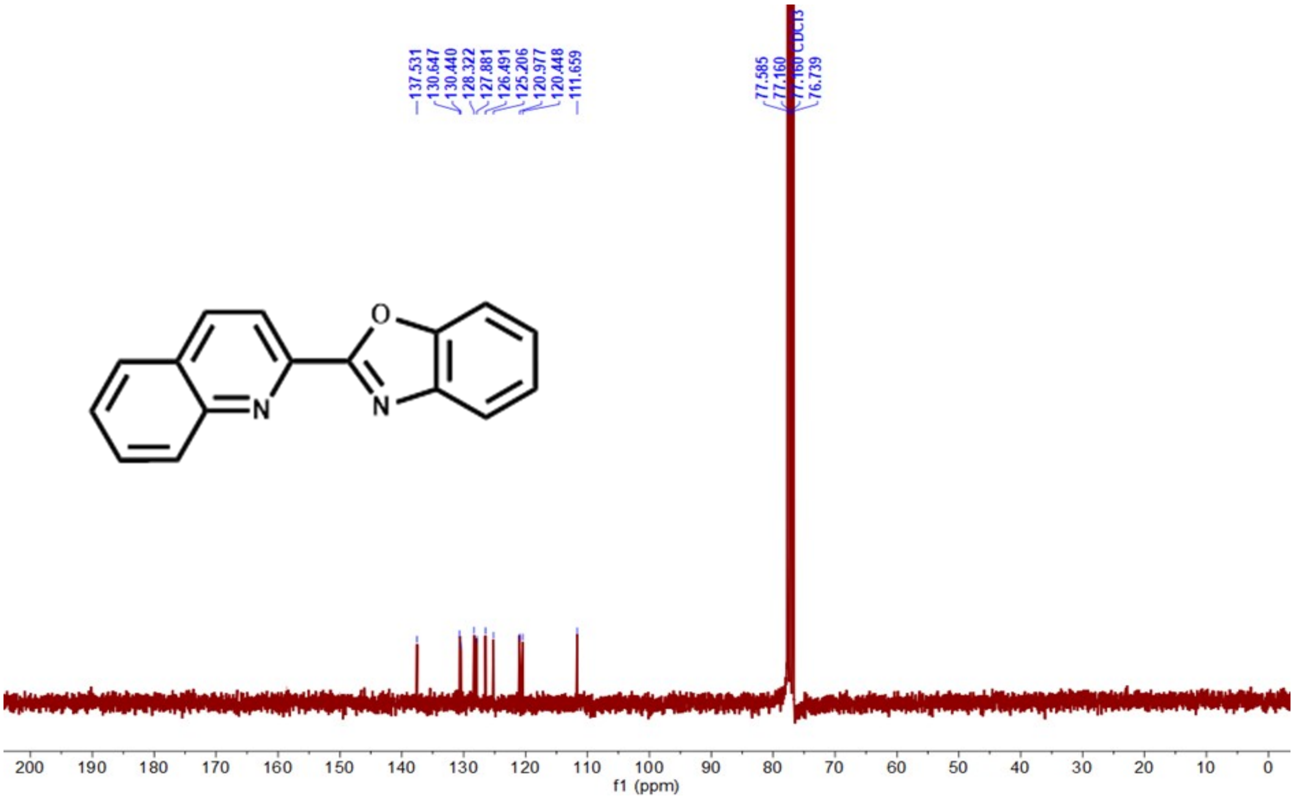

Fig. S8: ^{13}C NMR Spectrum of Ligand-2a in $CDCl_3$

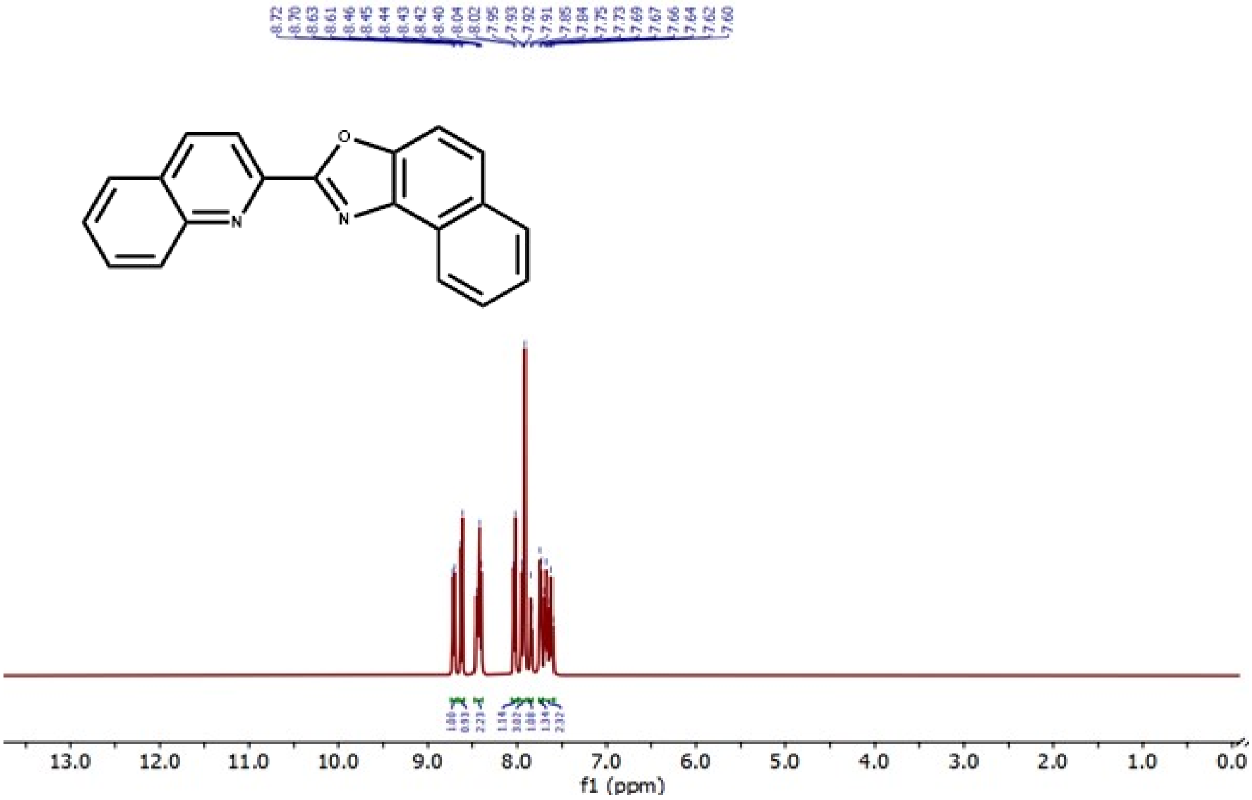

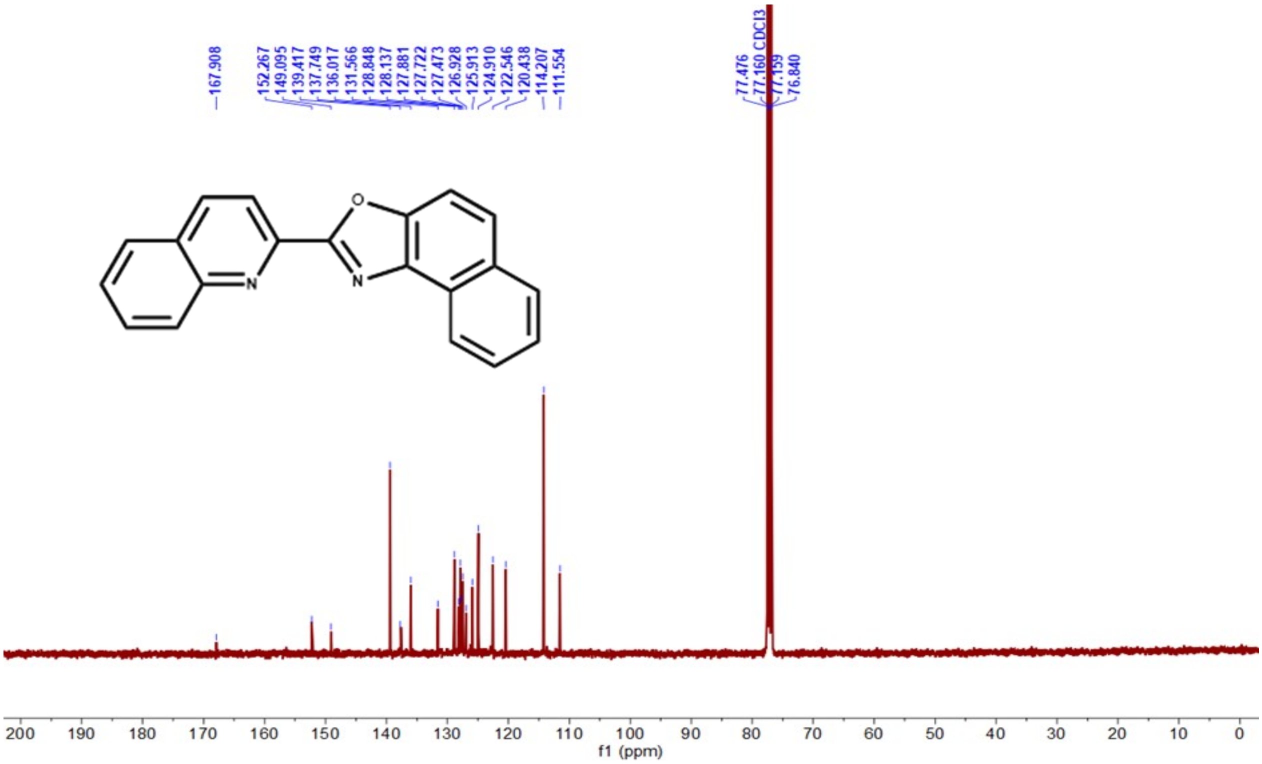

Fig. S9: ^{1}H NMR Spectrum of Ligand-2b in $CDCl_3$

Fig. S10: ^{13}C NMR Spectrum of Ligand-2b in $CDCl_3$

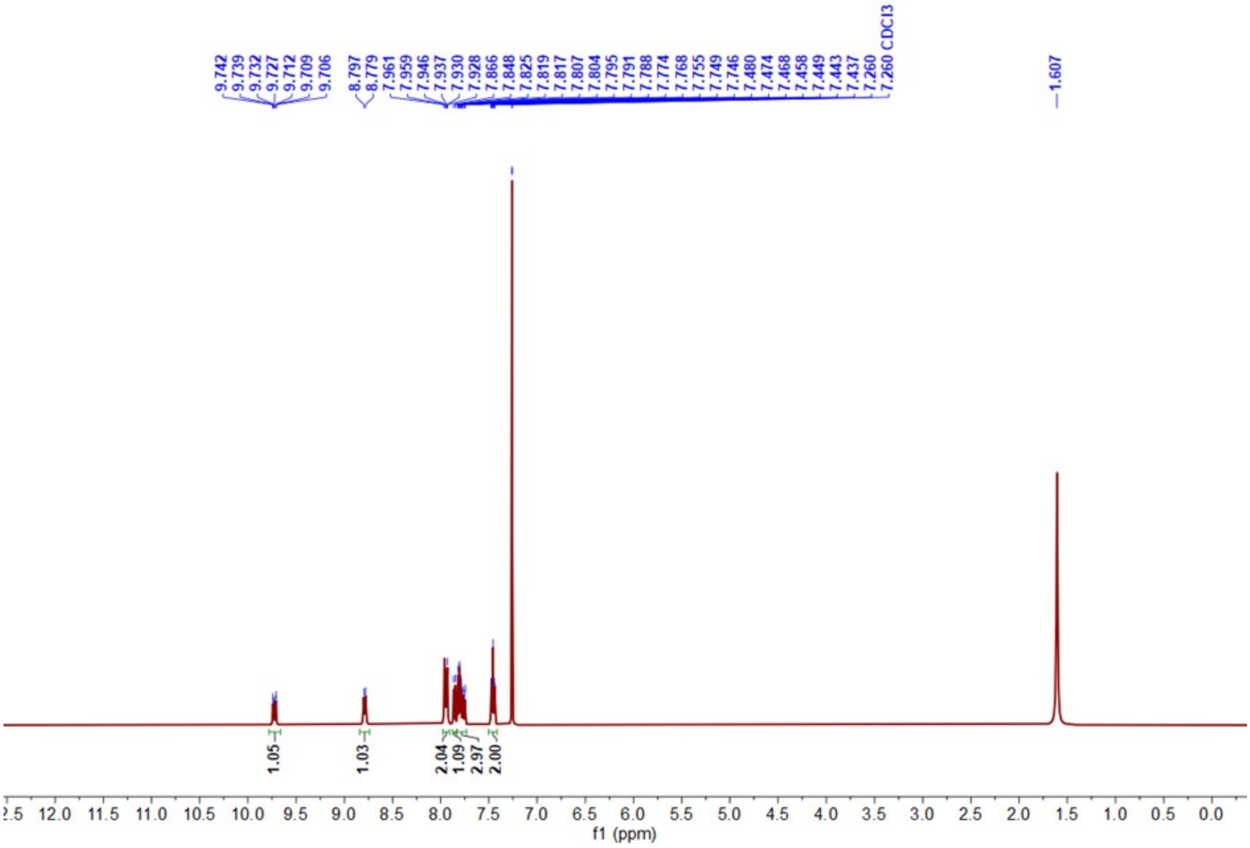

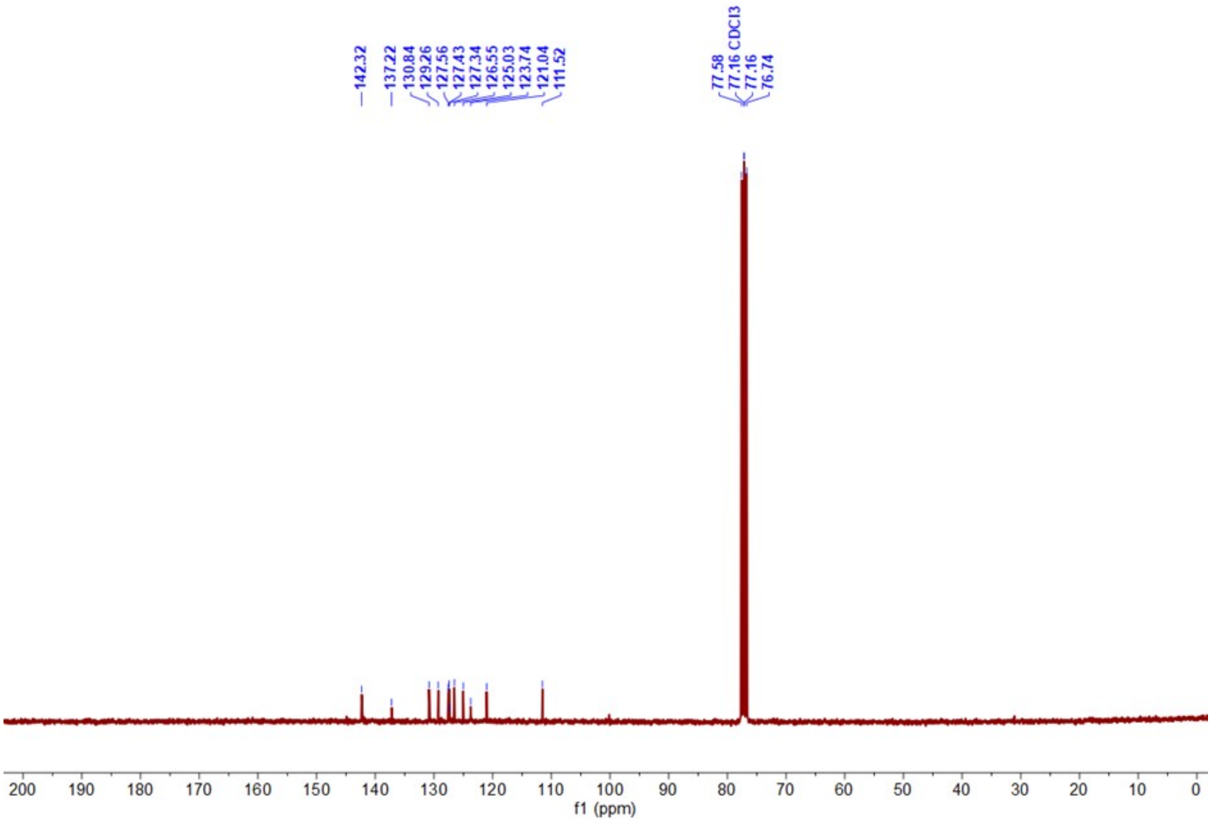

Fig. S11: ^{1}H NMR Spectrum of Ligand-3a in CDCl$_3$

Fig. S12: ^{13}C NMR Spectrum of Ligand-3a in CDCl$_3$

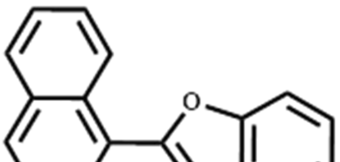

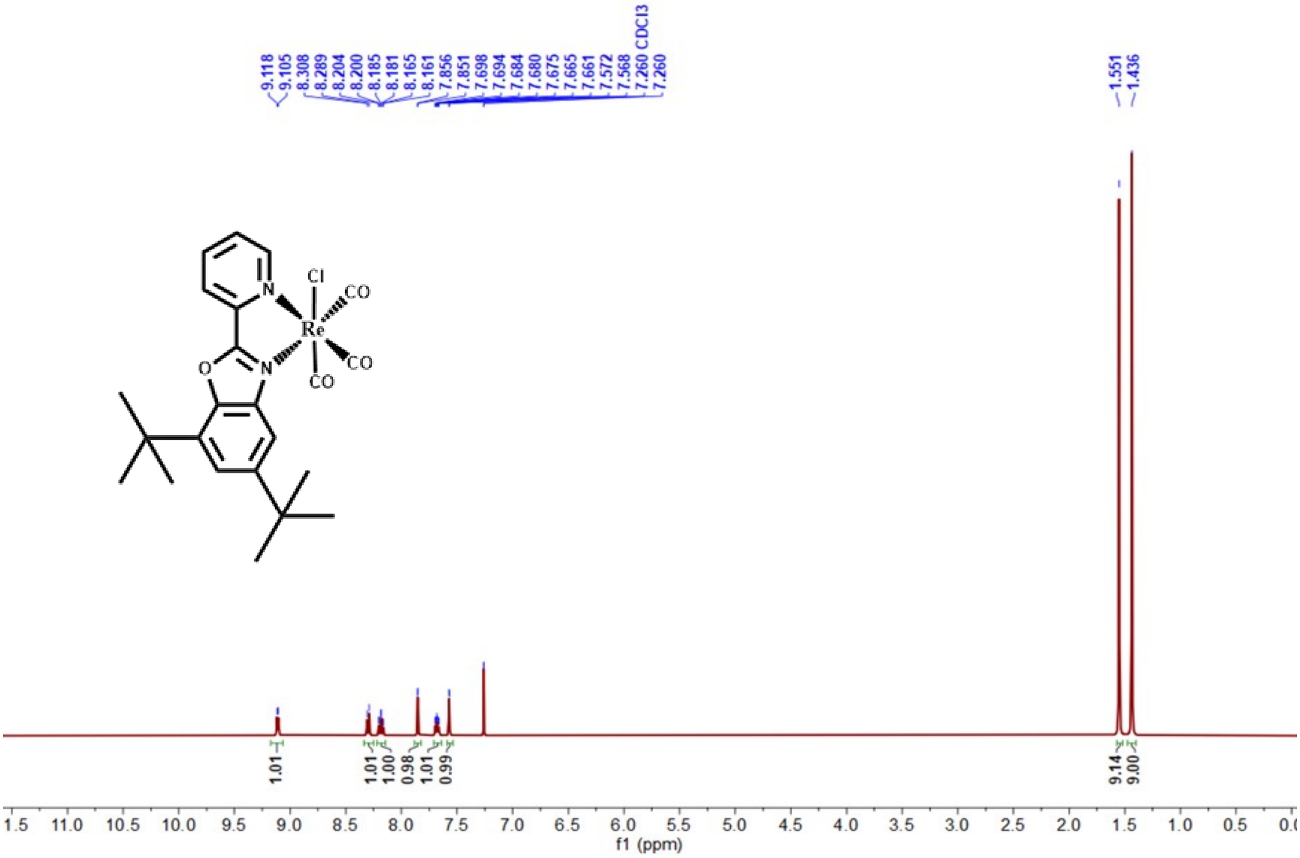

Fig. S13: ^{1}**H NMR Spectrum of Complex-1a in** $CDCl_3$

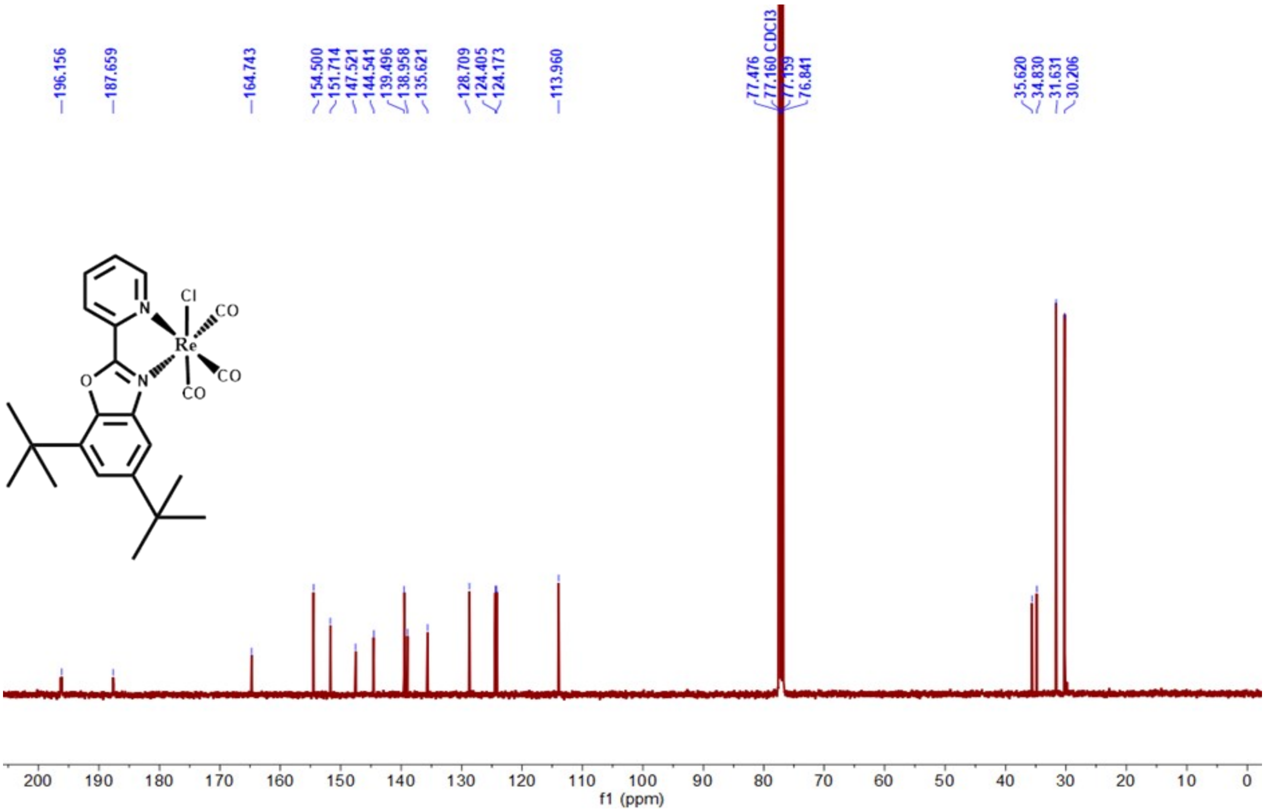

Fig. S14: ^{13}**C NMR Spectrum of Complex-1a in** $CDCl_3$**.**

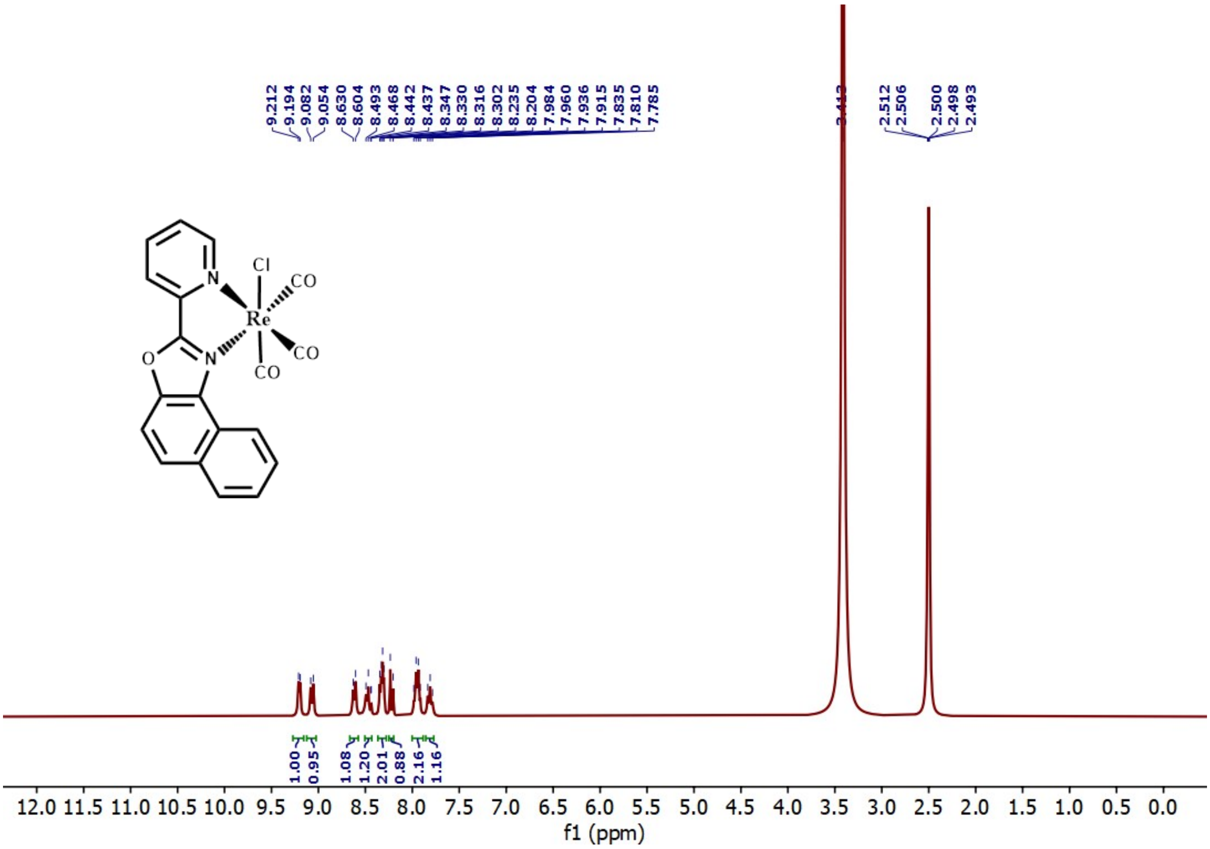

Fig. S15: ^{1}H NMR Spectrum of Complex-1b in DMSO-d$_6$

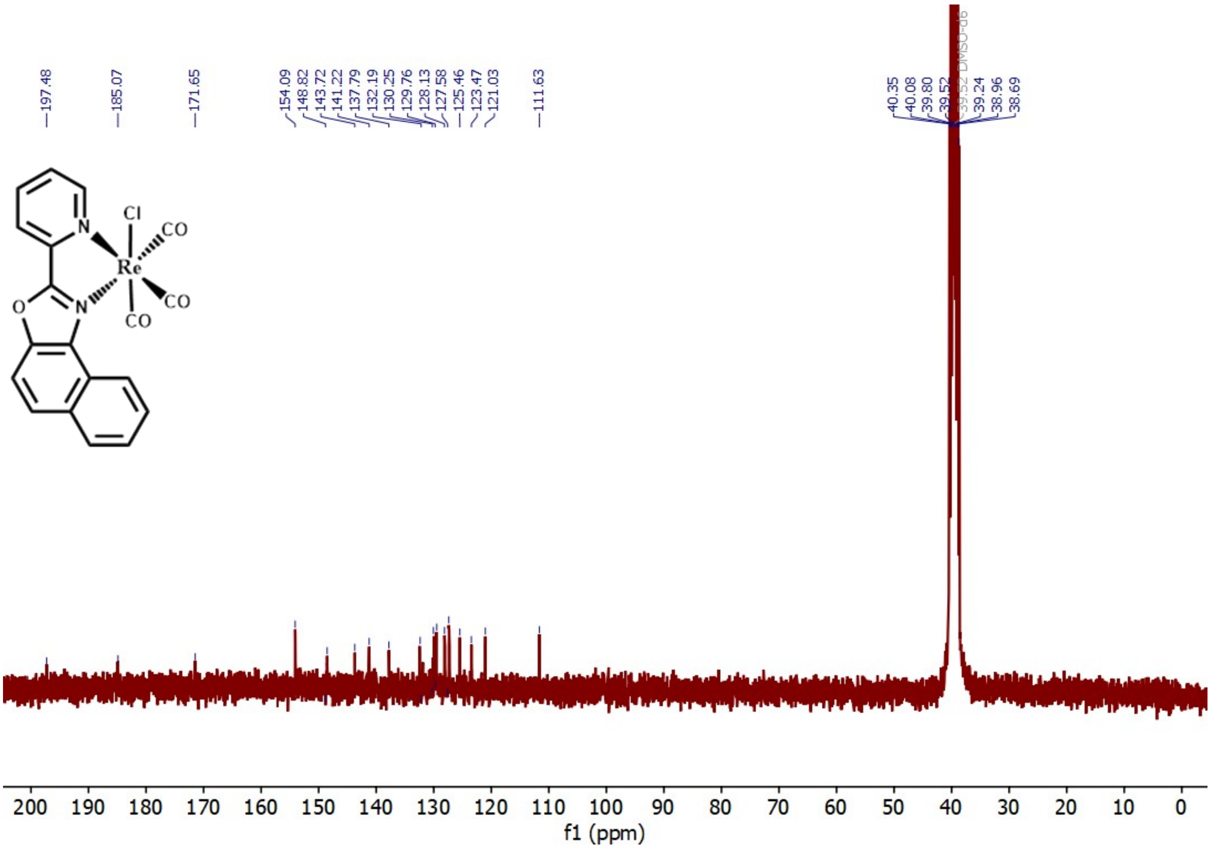

Fig. S16: ^{13}C NMR Spectrum of Complex-1b in DMSO-d$_6$

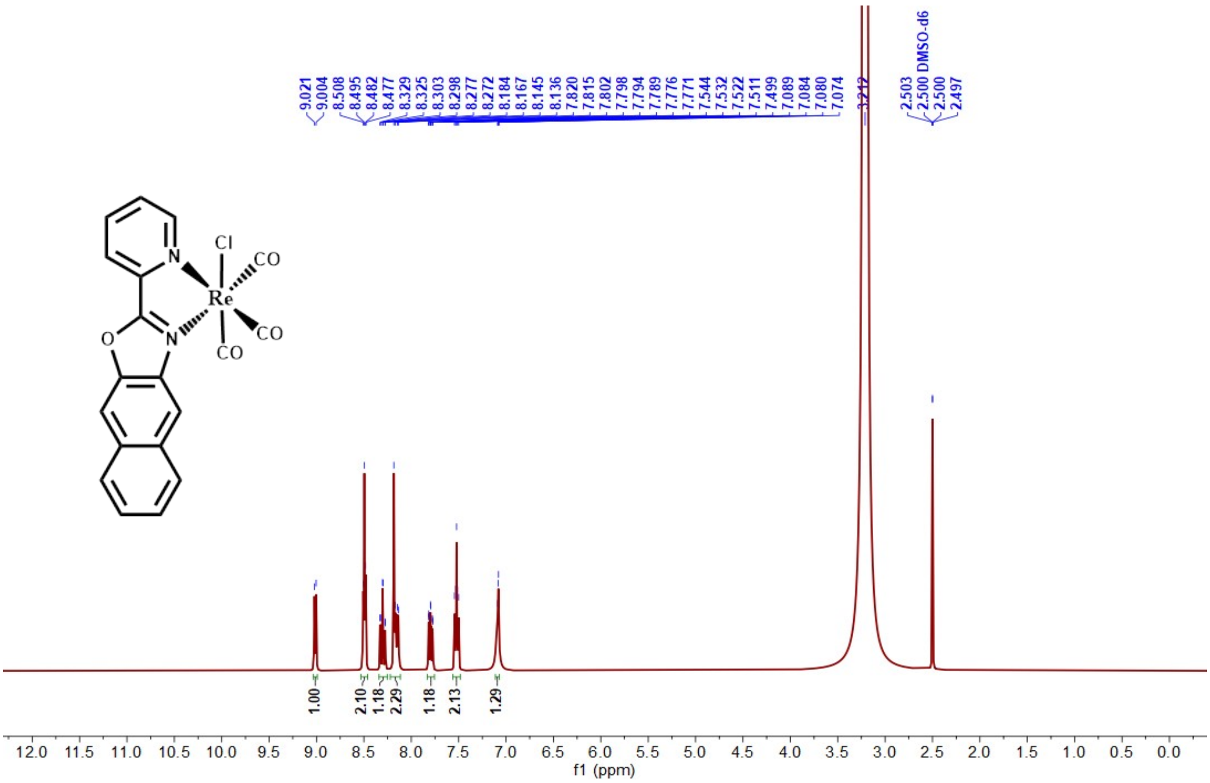

Fig. S17: ^{1}H NMR Spectrum of Complex-1c in DMSO-d$_6$

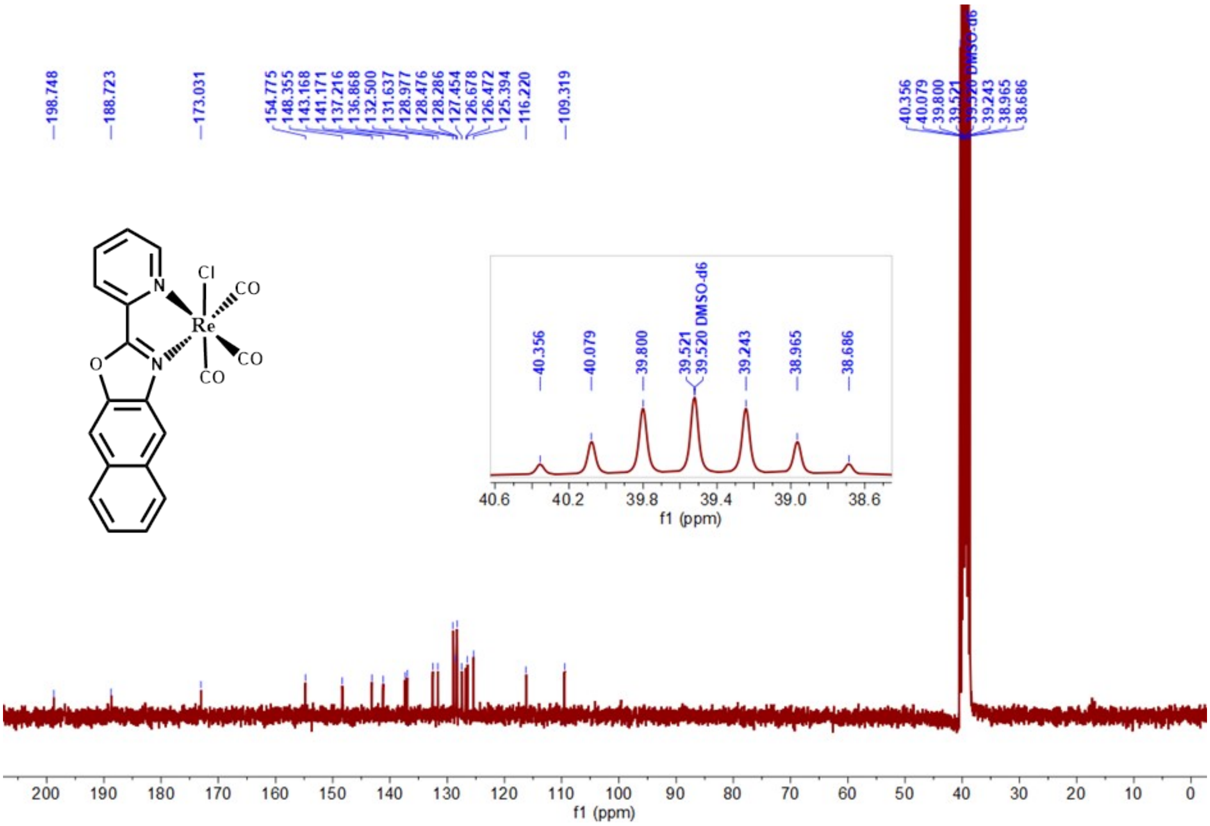

Fig. S18: ^{13}C NMR Spectrum of Complex-1c in DMSO-d$_6$

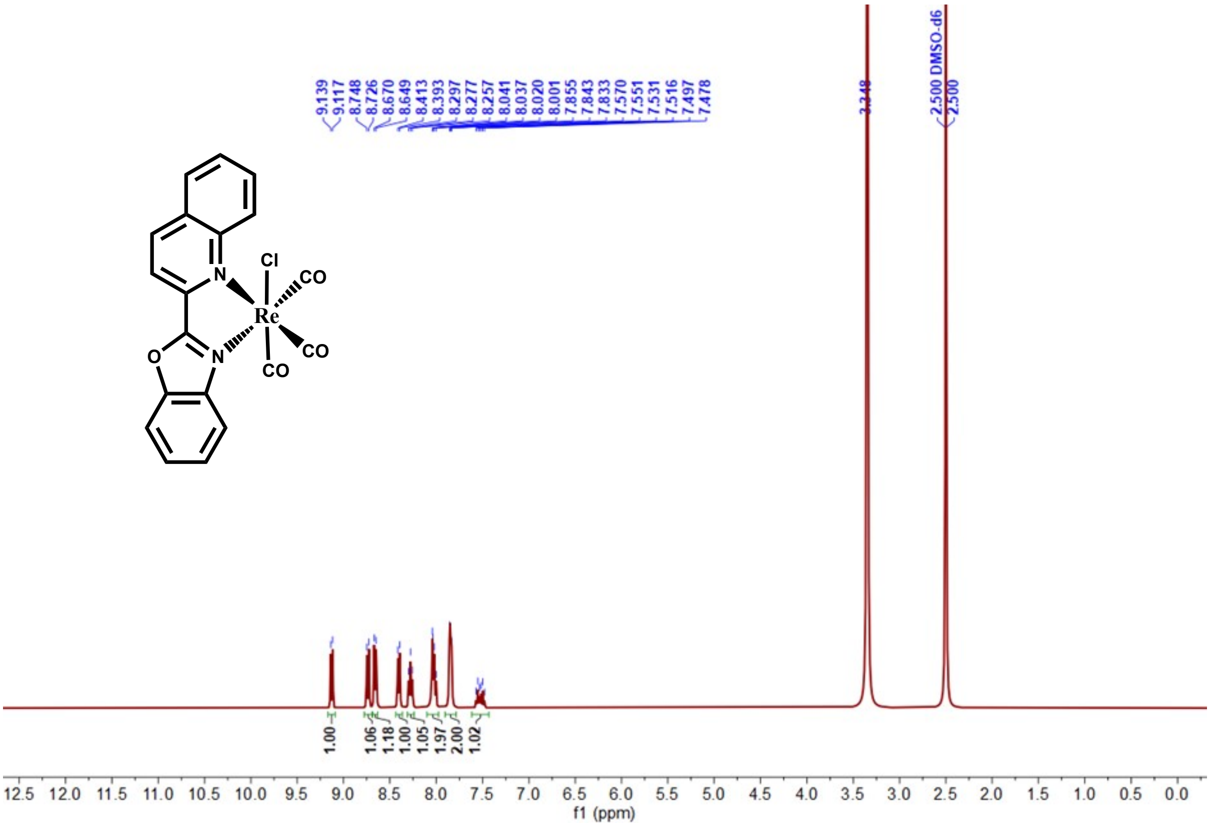

Fig. S19: ^{1}H NMR Spectrum of Complex-2a in DMSO-d$_6$

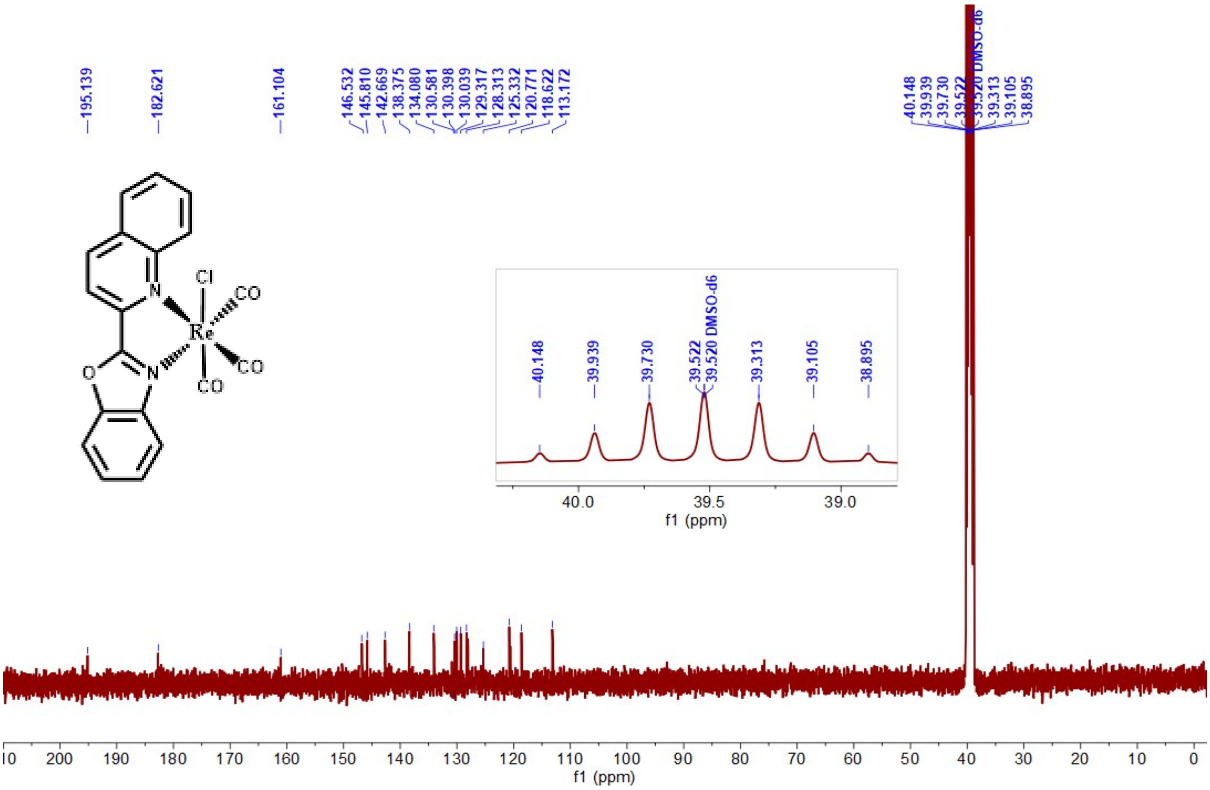

Fig. S20: ^{13}C NMR Spectrum of Complex-2a in DMSO-d_6

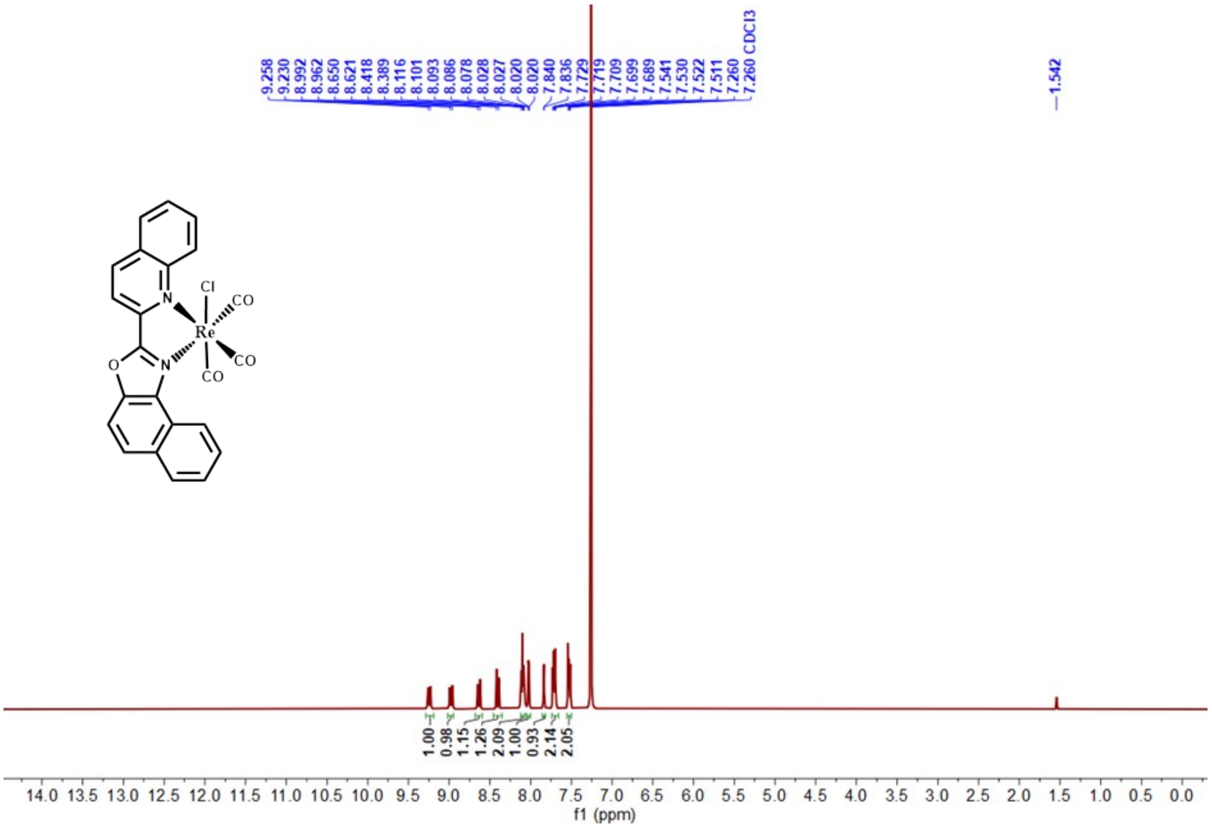

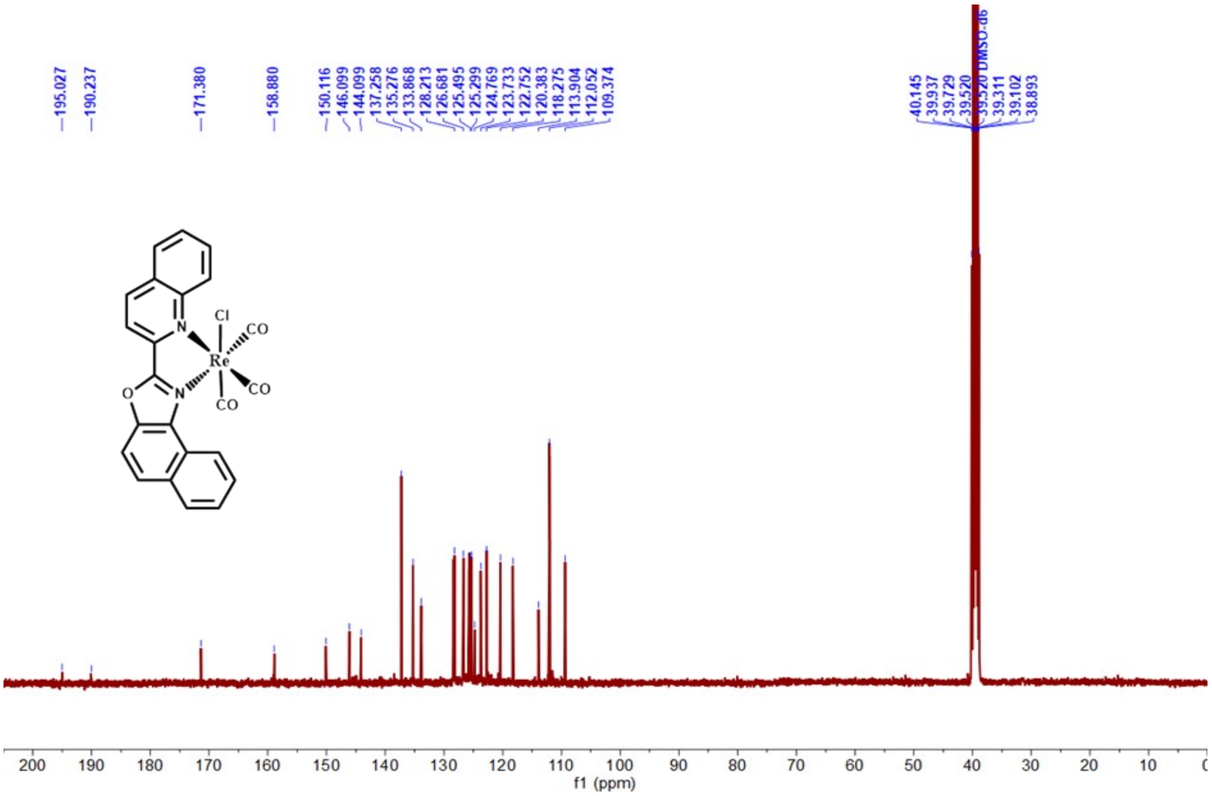

Fig. S21: ^{1}H NMR Spectrum of Complex-2b in DMSO-d$_{6}$.

Fig. S22: ^{13}C NMR Spectrum of Complex-2b in DMSO-d$_{6}$

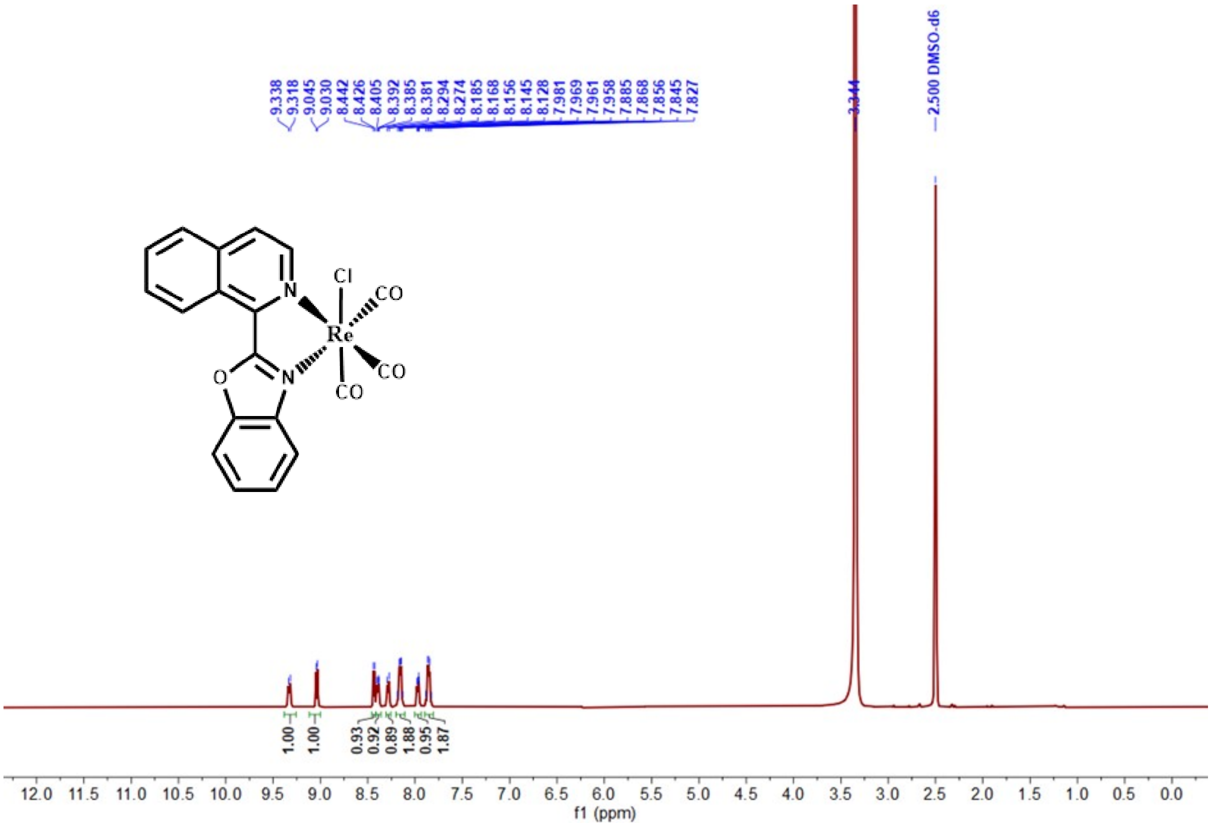

Fig. S23: ^{1}H NMR Spectrum of Complex-3a in DMSO-d$_{6}$.

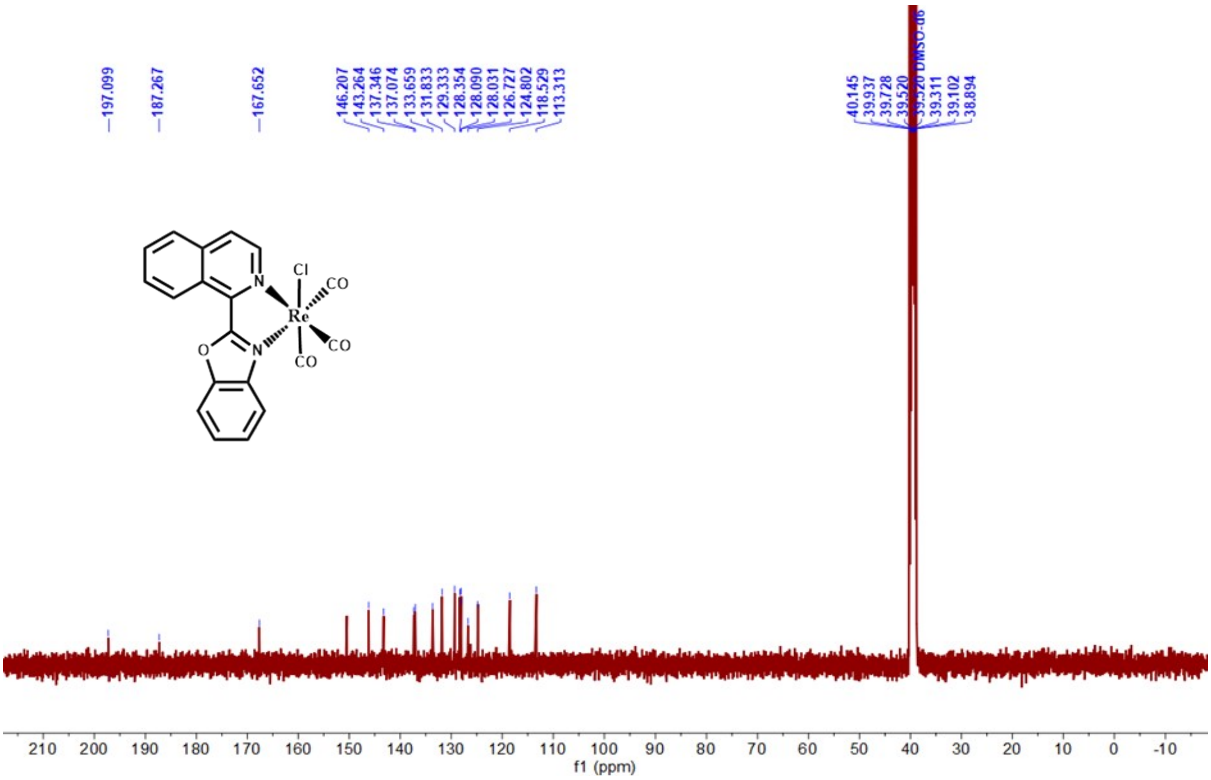

Fig. S24: ^{13}C NMR Spectrum of Complex-3a in DMSO-d$_{6}$

<table>
<tr><td colspan="2" rowspan="15">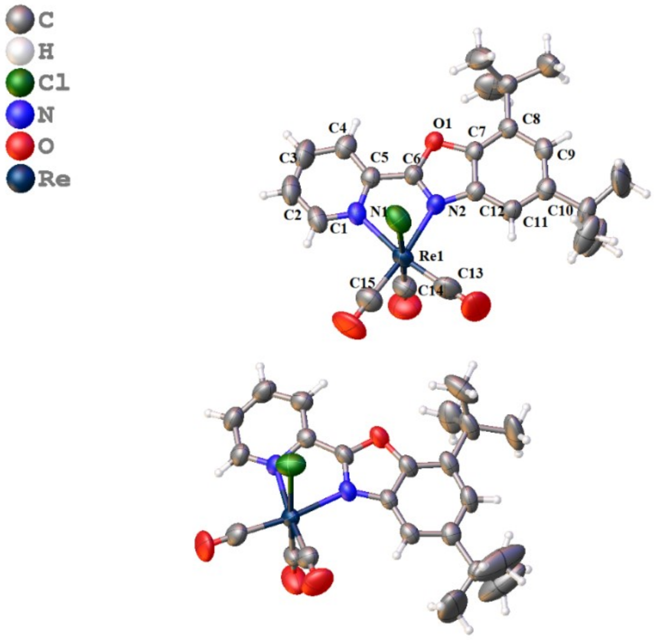 </td><td colspan="2">Complex-1a</td></tr>
<tr><td colspan="2">CCDC No. 2355624</td></tr>
<tr><td>Formula</td><td>$C_{45.75}H_{48}Cl_2N_4O_8Re_2$</td></tr>
<tr><td>Molecular weight</td><td>1225.18</td></tr>
<tr><td>Crystal system</td><td>monoclinic</td></tr>
<tr><td>Space group</td><td>P 1 21/c 1</td></tr>
<tr><td>a/ Å</td><td>16.2390(11)</td></tr>
<tr><td>b/ Å</td><td>11.9393(8)</td></tr>
<tr><td>c/ Å</td><td>26.1931(17)</td></tr>
<tr><td>α/°</td><td>90</td></tr>
<tr><td>β/°</td><td>105.713(2)</td></tr>
<tr><td>γ/°</td><td>90</td></tr>
<tr><td>V/ Å^3</td><td>4888.6(6)</td></tr>
<tr><td>Z</td><td>4</td></tr>
<tr><td>Dcalcd /g cm^{-3}</td><td>1.665</td></tr>
<tr><td colspan="2">Bond length(Å)</td><td>Mu (mm-1)</td><td>5.110</td></tr>
<tr><td>Re-N1</td><td>2.213(4)</td><td>T/K</td><td>273.15</td></tr>
<tr><td>Re-N2</td><td>2.170(4)</td><td colspan="2" rowspan="2">R1 = 0.0316,
wR2 = 0.0800</td></tr>
<tr><td>C6-O1</td><td>1.349(5)</td></tr>
<tr><td>O1-C7</td><td>1.395(5)</td><td>GOF on F2</td><td>1.056</td></tr>
<tr><td>C6-N2</td><td>1.308(6)</td><td colspan="2" rowspan="2"></td></tr>
<tr><td>N2-C12</td><td>1.399(6)</td></tr>
</table>

Table S1: crystallographic data of the **complex 1a**

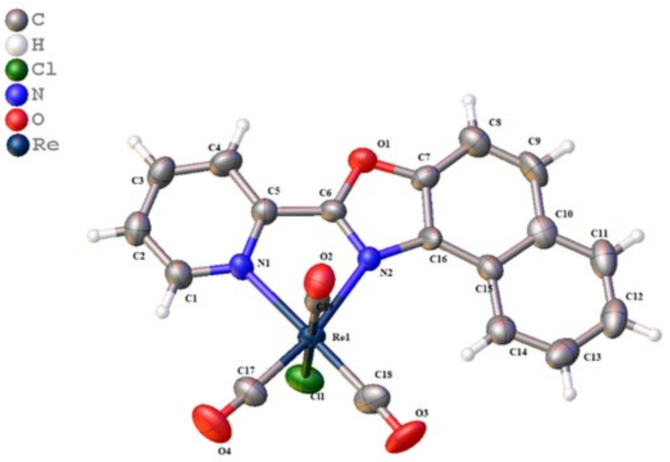		**Complex-1b**	
		CCDC No. 2385160	
		Formula	**$C_{19} H_{10} Cl N_2 O_4 Re$**
		Molecular weight	**551.94**
		Crystal system	**'triclinic'**
		Space group	**P -1**
		a/ Å	**6.977(5)**
		b/ Å	**9.781(7)**
		c/ Å	**13.71(1)**
		α/°	**86.855(19)**
		β/°	**75.528(18)**
		γ/°	**76.140(18)**
		V/ Å^3	**879.5(11)**
		Z	**2**
		Dcalcd /g cm^{-3}	**2.084**
Bond length(Å)		**Mu (mm-1)**	**7.088**
Re-N1	**2.211(6)**	**T/K**	**273**
Re-N2	**2.254(6)**	**R1 = 0.0488,** **wR2 = 0.1139**	
C6-O1	**1.349(8)**		
O1-C7	**1.377(9)**	**GOF on F2**	**1.074**
C6-N2	**1.315(8)**		
N2-C16	**1.411(9)**		

Table S2: crystallographic data of the **complex 1b**

<table>
<tr><td colspan="2" rowspan="15">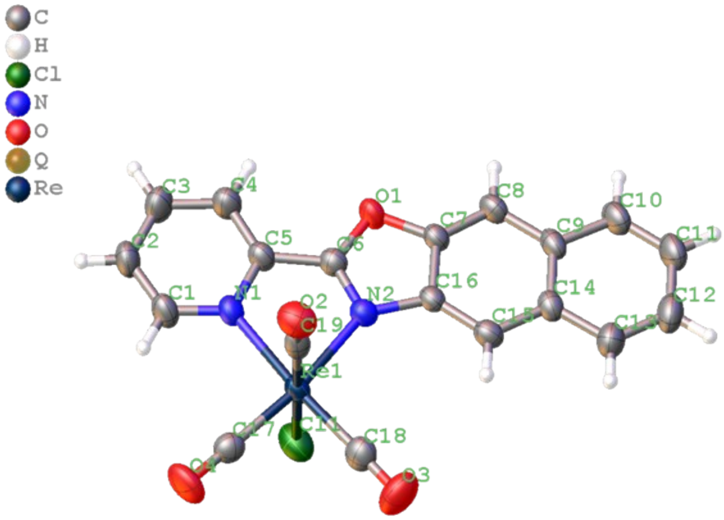 </td><td colspan="2">Complex-1c</td></tr>
<tr><td colspan="2">CCDC No. 2385164</td></tr>
<tr><td>Formula</td><td>$C_{19}H_{10}ClN_2O_4Re$, 1[CH_2Cl_2]</td></tr>
<tr><td>Molecular weight</td><td>636.87</td></tr>
<tr><td>Crystal system</td><td>'triclinic'</td></tr>
<tr><td>Space group</td><td>P -1</td></tr>
<tr><td>a/ Å</td><td>9.4862(4)</td></tr>
<tr><td>b/ Å</td><td>9.5540(4)</td></tr>
<tr><td>c/ Å</td><td>13.1539(6)</td></tr>
<tr><td>α/°</td><td>96.340(1)</td></tr>
<tr><td>β/°</td><td>102.856(1)</td></tr>
<tr><td>γ/°</td><td>110.709(1)</td></tr>
<tr><td>V/ $Å^3$</td><td>1063.54(8)</td></tr>
<tr><td>Z</td><td>2</td></tr>
<tr><td>Dcalcd /g cm^{-3}</td><td>1.989</td></tr>
<tr><td colspan="2">Bond length(Å)</td><td>Mu/mm^{-1}</td><td>6.119</td></tr>
<tr><td>Re-N1</td><td>2.205(3)</td><td>T/K</td><td>273</td></tr>
<tr><td>Re-N2</td><td>2.179(3)</td><td colspan="2" rowspan="2">R1 = 0.0252,
wR2 = 0.0550</td></tr>
<tr><td>C6-O1</td><td>1.352(5)</td></tr>
<tr><td>O1-C7</td><td>1.390(5)</td><td>GOF on F2</td><td>0.983</td></tr>
<tr><td>C6-N2</td><td>1.293(5)</td><td colspan="2" rowspan="2"></td></tr>
<tr><td>N2-C16</td><td>1.417(5)</td></tr>
</table>

Table S3: crystallographic data of the complex **1c**

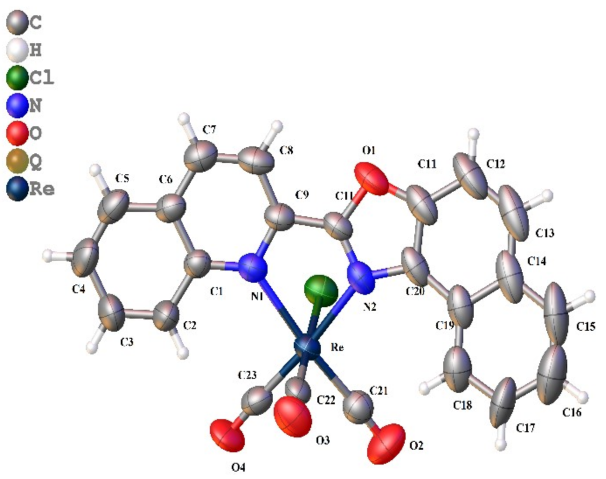

Complex-2b	
CCDC No. 2385178	
Formula	**C23 H12 Cl N2 O4 Re**
Molecular weight	**602.00**
Crystal system	**'monoclinic'**
Space group	**P -1**
a/ Å	**7.2623(6)**
b/ Å	**9.6207(7)**
c/ Å	**14.8789(11)**
α/°	**99.464(2)**
β/°	**96.228(3)**
γ/°	**100.601(2)**
V/ Å^3	**997.54(13)**
Z	**2**
Dcalcd /g cm^{-3}	**2.004**
Mu/mm^{-1}	**6.259**
T/K	**273**
R1 = 0.0400, **wR2 = 0.1004**	
GOF on F2	**1.047**

Bond length(Å)	
Re-N1	**2.279(6)**
Re-N2	**2.209(6)**
C10-O1	**1.362(8)**
O1-C11	**1.376(12)**
C10-N2	**1.279(10)**
N2-C20	**1.396(10)**

Table S4: crystallographic data of the **complex-2b**

<table>
<tr><td colspan="2" rowspan="15">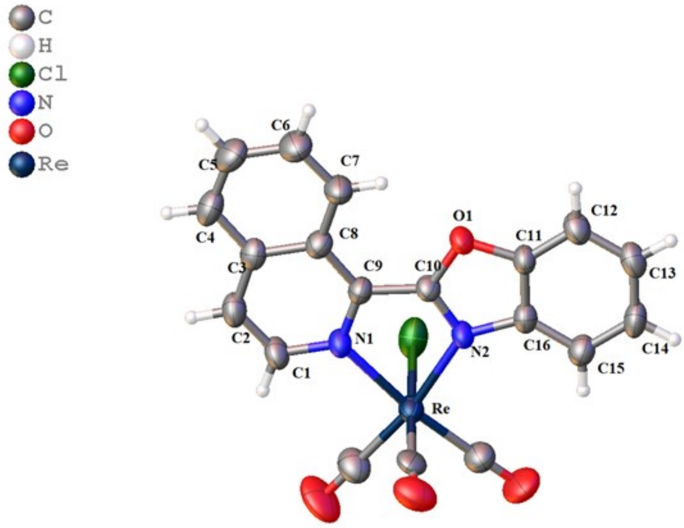 </td><td colspan="2">Complex-3a</td></tr>
<tr><td colspan="2">CCDC No. 2385175</td></tr>
<tr><td>Formula</td><td>C19 H10 Cl N2 O4 Re</td></tr>
<tr><td>Molecular weight</td><td>551.94</td></tr>
<tr><td>Crystal system</td><td>'monoclinic'</td></tr>
<tr><td>Space group</td><td>'P 1 21/c 1'</td></tr>
<tr><td>a/ Å</td><td>8.3981(5)</td></tr>
<tr><td>b/ Å</td><td>16.0907(9)</td></tr>
<tr><td>c/ Å</td><td>13.2068(8)</td></tr>
<tr><td>α/°</td><td>90</td></tr>
<tr><td>β/°</td><td>93.733(2)</td></tr>
<tr><td>γ/°</td><td>90</td></tr>
<tr><td>V/ $Å^3$</td><td>1780.87(18)</td></tr>
<tr><td>Z</td><td>4</td></tr>
<tr><td>Dcalcd /g cm^{-3}</td><td>2.059</td></tr>
<tr><td colspan="2">Bond length(Å)</td><td>Mu/mm^{-1}</td><td>7.002</td></tr>
<tr><td>Re-N1</td><td>2.210(5)</td><td>T/K</td><td>273</td></tr>
<tr><td>Re-N2</td><td>2.158(4)</td><td colspan="2" rowspan="2">R1 = 0.0346,
wR2 = 0.0976</td></tr>
<tr><td>C10-O1</td><td>1.350(6)</td></tr>
<tr><td>O1-C11</td><td>1.391(6)</td><td>GOF on F2</td><td>1.059</td></tr>
<tr><td>C10-N2</td><td>1.350(6)</td><td colspan="2" rowspan="2"></td></tr>
<tr><td>N2-C16</td><td>1.401(7)</td></tr>
</table>

Table S5: crystallographic data of the complex-3a

Vibrational Spectra

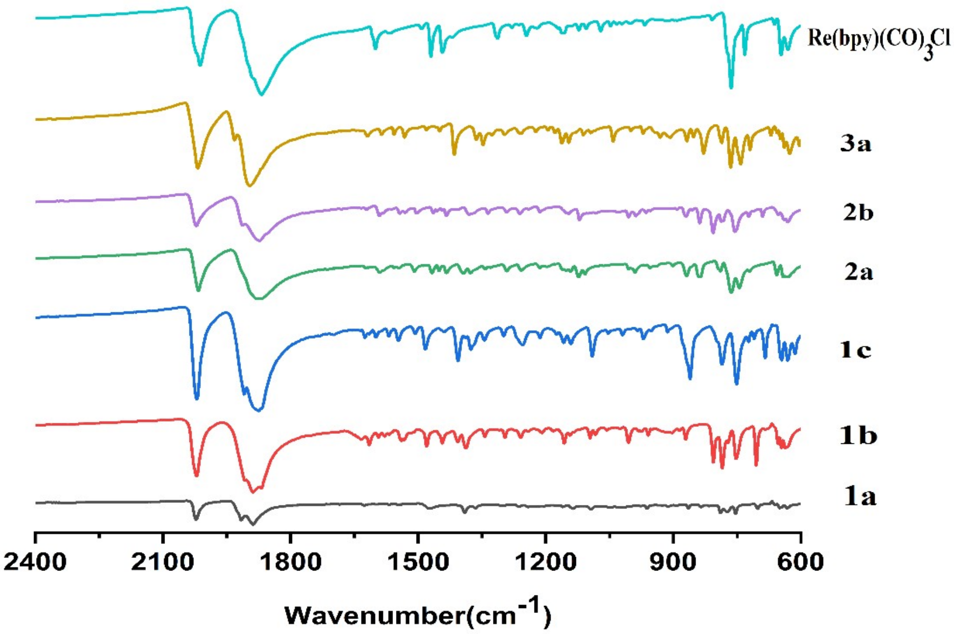

Fig. S25: FTIR Spectra of the complexes.

complex	experimental ν_{CO} (cm^{-1})
Re(bpy)(CO)$_3$Cl	**2021, 1917, 1897**
Complex-1a	**2021, 1915, 1888**
Complex-1b	**2020, 1906, 1880**
Complex-1c	**2020, 1908, 1883**
Complex-2a	**2016, 1915, 1879**
Complex-2b	**2021, 1912, 1876**
Complex-3a	**2018, 1931, 1896**

Table S6: IR stretching frequencies of the complexes.

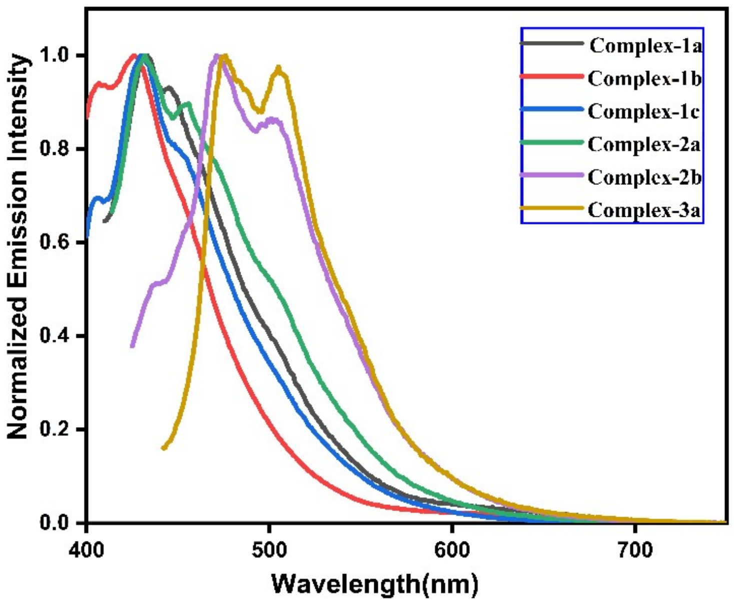

Fig. S26: Normalized Emission plots of the complexes (1a, 1b, 1c, 2a, 2b, 3a) recorded in CH_3CN at room temperature.

Complex	λ_{exc}(nm)	λ_{emi}(nm)	Φ_{EM}	τ_1(ns)	τ_2(ns)	τ_{avg}(ns)	$k_r(s^{-1})\times10^7$	$k_{nr}(s^{-1})\times10^8$
1a	400	431,446	0.11	1.32	7.73	4.17	1.4	1.15
1b	400	405,424	0.51	2.11	-	2.11	24.1	2.32
1c	402	429	0.24	1.54	7.72	5.27	3.1	0.98
2a	400	431,455	0.13	1.87	7.48	7.06	1.7	1.26
2b	416	471,501	0.07	2.02	-	2.02	3.4	4.6
3c	430	474,504	0.05	2.04	8.17	5.28	0.6	1.16

Table S7: Photophysical parameters of the complexes. All the complexes were excited at the maximum wavelength of absorption (λ_{max}=λ_{exc})

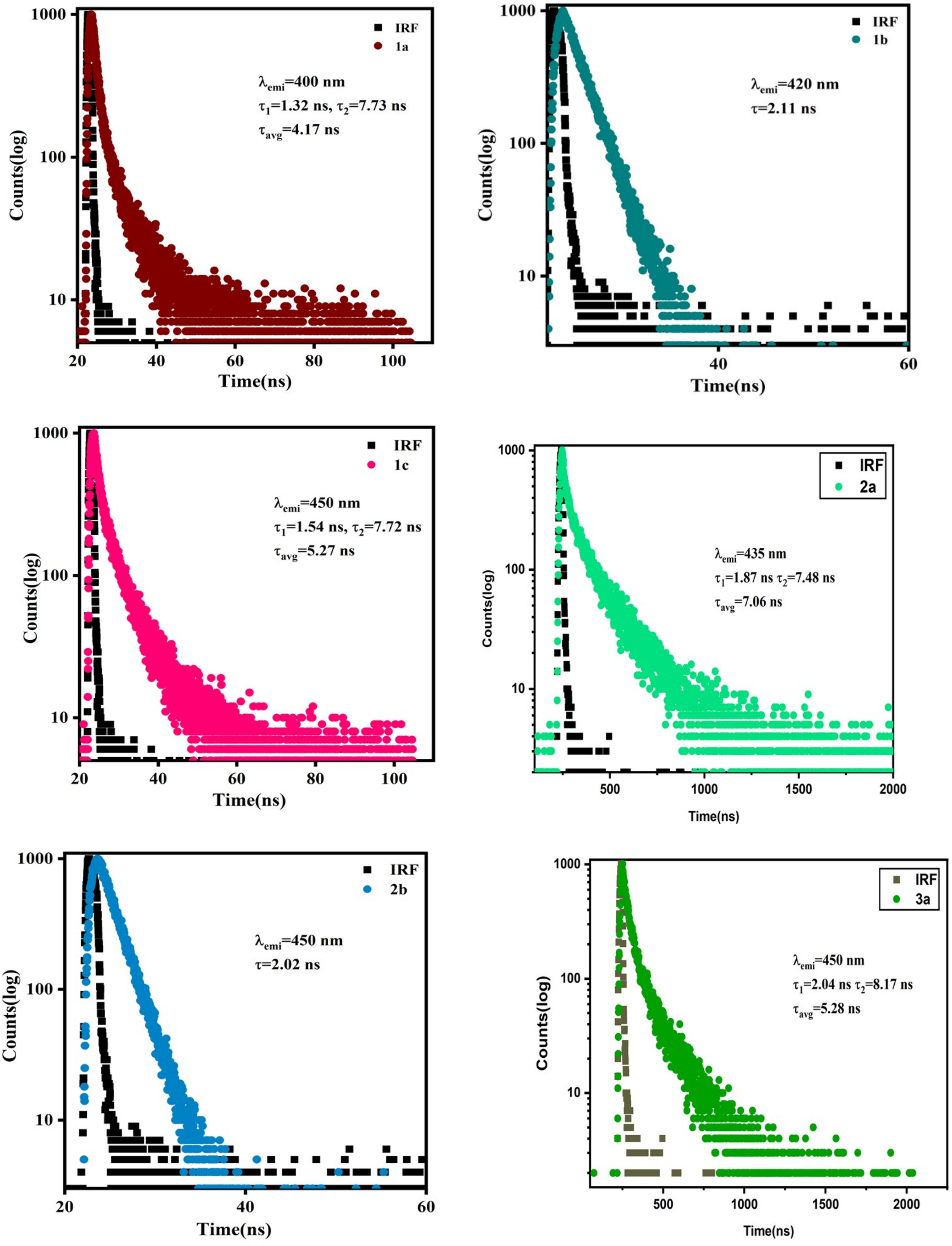

Fig. S27. Emission decay curves of **complex-1a, 1b, 1c, 2a, 2b and 3a** in aerated CH_3CN.

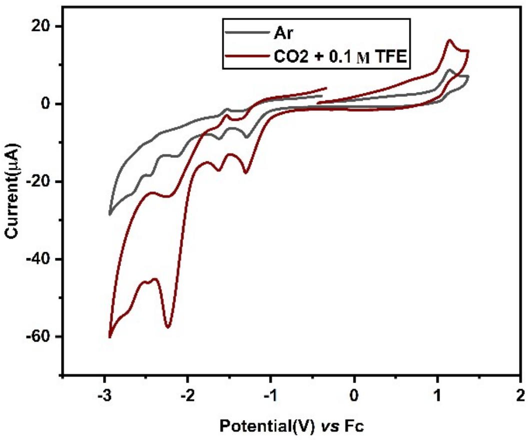

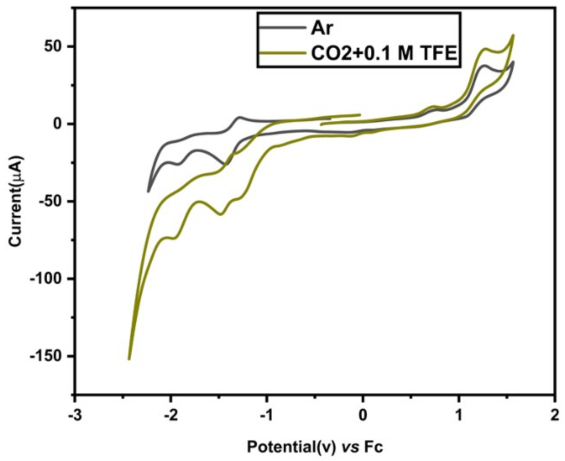

Electrochemistry

1a

1c

2a

2b

3a

Fig. S28: Cyclic voltammograms of 1 mM solution of **complexes 1a, 1b, 1c, 2a, 2b** and **3a** under Ar (black) and CO_2 atmosphere. Potential values are reported versus Fc^+/Fc.

Calculation of TOF_{max} for the Complexes:

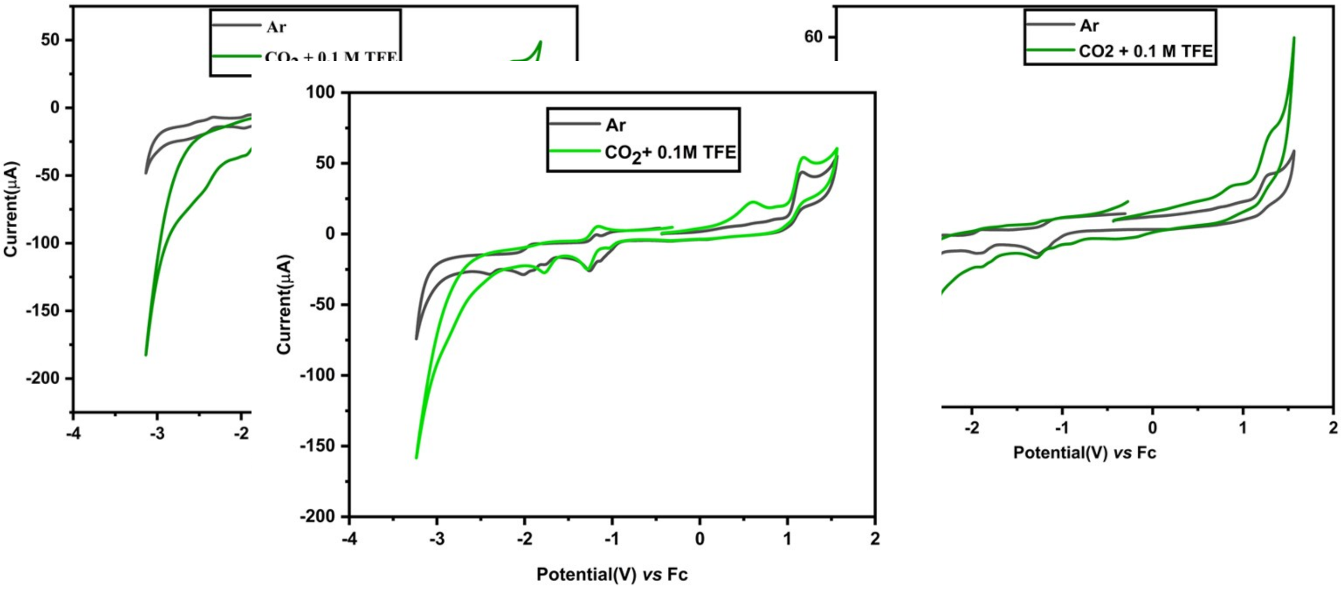

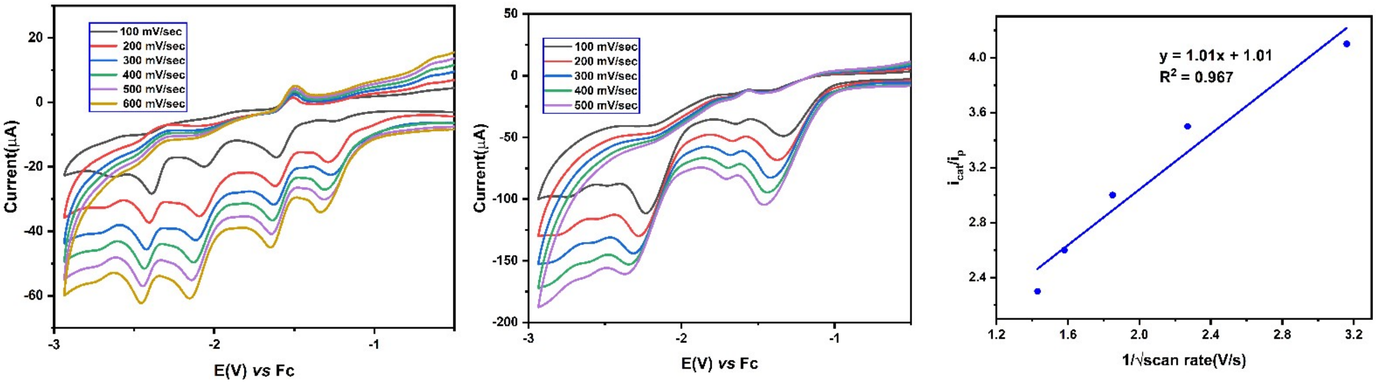

(a) **(b)** **(c)**

Fig. S29: Current *vs.* potential plot in different scan rate in Ar **(a)** and in presence of CO_2 **(b)**. ip/icat vs. 1/scan rate$^{1/2}$ plot Complex 1a. Cyclic voltammogram scan rate dependence of 1 mM **complex-1a** under an atmosphere of argon **(a)** and under an atmosphere of CO_2 **(b)** in acetonitrile. **(c)** i_p/i_{cat} vs. 1/scan rate$^{1/2}$ plot of **complex-1a**. Electrochemical conditions were 0.1 M TBAH as supporting electrolyte, 3 mm diameter glassy carbon working electrode, Pt wire counter electrode, and Ag/AgCl reference electrode.

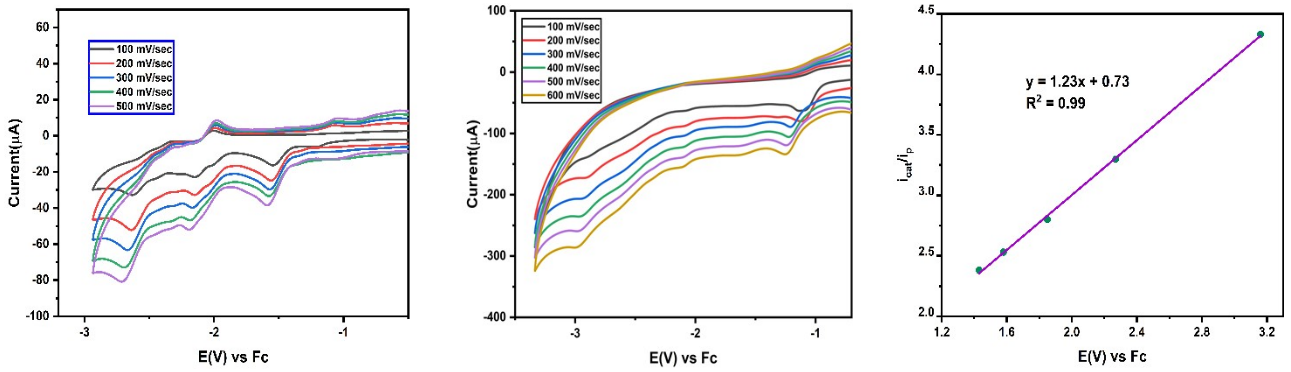

(a) **(b)** **(c)**

Fig. S30: Current *vs.* potential plot in different scan rate in Ar **(a)** and in presence of CO_2 **(b)**. ip/icat vs. 1/scan rate$^{1/2}$ plot Complex 1a. Cyclic voltammogram scan rate dependence of 1 mM **complex-1b** under an atmosphere of argon **(a)** and under an atmosphere of CO_2 **(b)** in acetonitrile. **(c)** i_p/i_{cat} vs. 1/scan rate$^{1/2}$ plot of **complex-1b**. Electrochemical conditions were 0.1 M TBAH as supporting electrolyte, 3 mm diameter glassy carbon working electrode, Pt wire counter electrode, and Ag/AgCl reference electrode.

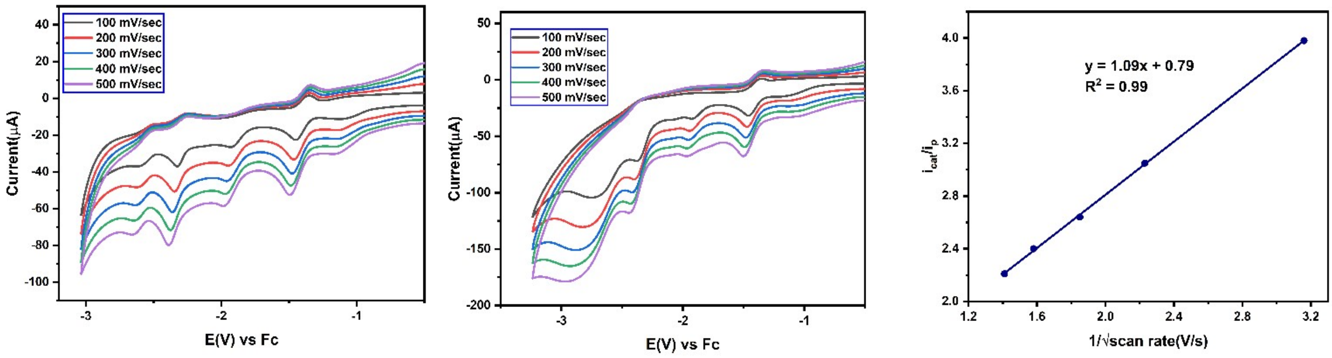

(a) **(b)** **(c)**

Fig. S31: Current *vs.* potential plot in different scan rate in Ar **(a)** and in presence of CO_2 **(b)**. ip/icat vs. 1/scan rate$^{1/2}$ plot Complex 1a. Cyclic voltammogram scan rate dependence of 1 mM **complex-1c** under an atmosphere of argon **(a)** and under an atmosphere of CO_2 **(b)** in acetonitrile. **(c)** i_p/i_{cat} vs. 1/scan rate$^{1/2}$ plot of **complex-1c**. Electrochemical conditions were 0.1 M TBAH as supporting electrolyte, 3 mm diameter glassy carbon working electrode, Pt wire counter electrode, and Ag/AgCl reference electrode.

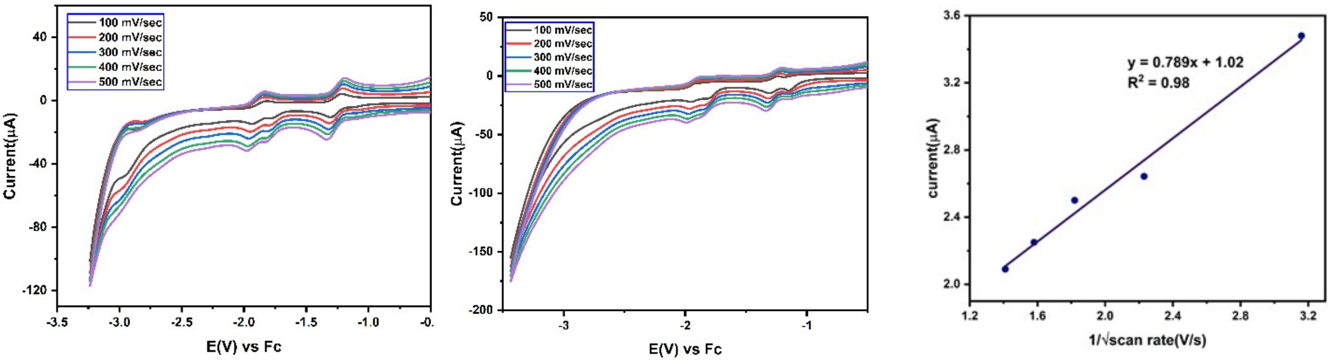

(a) **(b)** **(c)**

Fig. S32: Current *vs.* potential plot in different scan rate in Ar **(a)** and in presence of CO_2 **(b)**. ip/icat vs. 1/scan rate$^{1/2}$ plot Complex 1a. Cyclic voltammogram scan rate dependence of 1 mM **complex-2a** under an atmosphere of argon **(a)** and under an atmosphere of CO_2 **(b)** in acetonitrile. **(c)** i_p/i_{cat} vs. 1/scan rate$^{1/2}$ plot of **complex-2a**. Electrochemical conditions were 0.1 M TBAH as supporting electrolyte, 3 mm diameter glassy carbon working electrode, Pt wire counter electrode, and Ag/AgCl reference electrode.

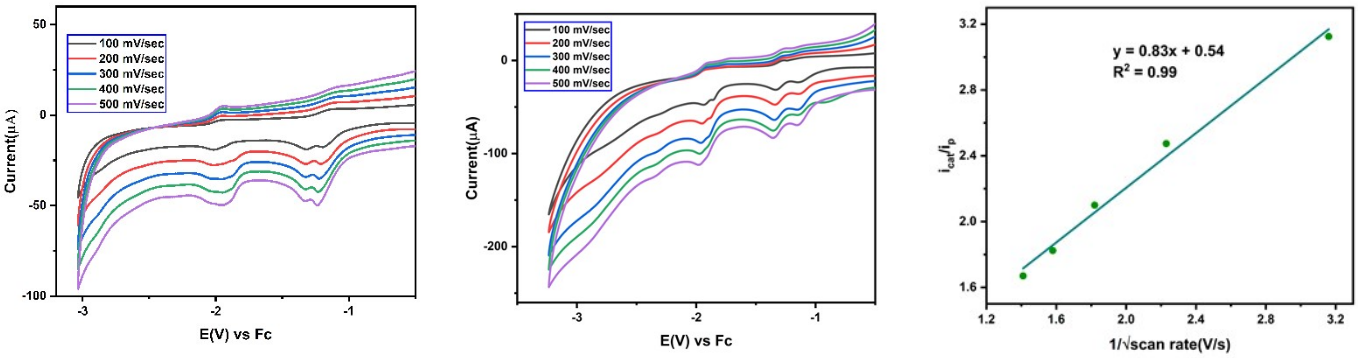

(a) (b) (c)

Fig. S33: Current *vs.* potential plot in different scan rate in Ar **(a)** and in presence of CO_2 **(b)**. ip/icat vs. 1/scan rate$^{1/2}$ plot Complex 1a. Cyclic voltammogram scan rate dependence of 1 mM **complex-2b** under an atmosphere of argon **(a)** and under an atmosphere of CO_2 **(b)** in acetonitrile. **(c)** i_p/i_{cat} vs. 1/scan rate$^{1/2}$ plot of **complex-2b**. Electrochemical conditions were 0.1 M TBAH as supporting electrolyte, 3 mm diameter glassy carbon working electrode, Pt wire counter electrode, and Ag/AgCl reference electrode.

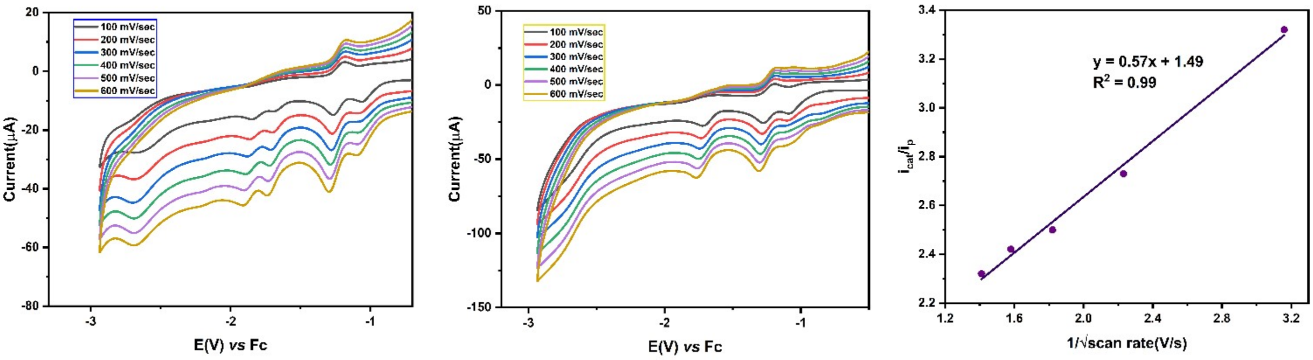

(a) (b) (c)

Fig. S34: Current *vs.* potential plot in different scan rate in Ar **(a)** and in presence of CO_2 **(b)**. i_p/i_{cat} vs. 1/scan rate$^{1/2}$ plot Complex 1a. Cyclic voltammogram scan rate dependence of 1 mM **complex-3a** under an atmosphere of argon **(a)** and under an atmosphere of CO_2 **(b)** in acetonitrile. **(c)** i_p/i_{cat} vs. 1/scan rate$^{1/2}$ plot of **complex-3a**. Electrochemical conditions were 0.1 M TBAH as supporting electrolyte, 3 mm diameter glassy carbon working electrode, Pt wire counter electrode, and Ag/AgCl reference electrode.

TOF_{max} calculations from the cyclic voltammetry experiments:

The turnover frequency (TOF) is an inherent characteristic of catalysts, which represents the rate of conversion reactants into products per mole of active catalyst per unit time. The TOF value was derived using the following equation below from the catalytic cyclic voltammograms recorded CH_3CN solutions.

$$TOF = (F\nu n_p^3/RT)(0.4463/n_{cat})(i_{cat}/i_p)^2$$

Where, i_p is peak current, i_{cat} is the catalytic current, F is Faraday's constant (F = 96500 C), R is the universal gas constant ($R = 8.314\ J\ K^{-1}\ mol^{-1}$), T is temperature (T = 300 K) and ν is the scan rate. (where n_p is 1, the number of electrons transferred in the noncatalytic reduction, and n_{cat} is 2 for CO_2 reduction to CO, the number of electrons transferred in the catalytic reaction). The TOF was calculated from the slope of i_{cat}/i_pvs $\nu^{-1/2}$ plot.

Catalyst	**TOF_{max}**
1a	$1.80\ s^{-1}$
1b	$2.90\ s^{-1}$
1c	$2.28\ s^{-1}$
2a	$1.19\ s^{-1}$
2b	$1.32\ s^{-1}$
3a	$0.62\ s^{-1}$

Table S8: $TOF_{max}$of the complexes in CH_3CN.

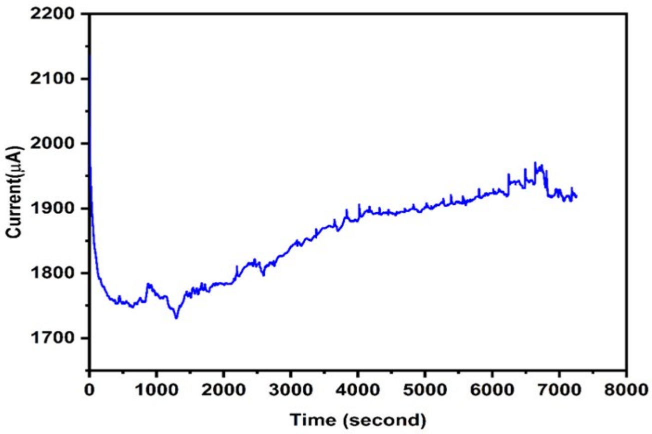

Fig. S35. Representative current versus time plots for controlled potential electrolyses of **Complex-1b**

Compound	Conc.(mM)	Faradaic efficiency (%)		
		H_2	CO	CH_4
1b	1	<1	33	6

Table S9. Faradaic efficiencies, in CH_3CN and 0.1M TFE after CPE experiments with a carbon working electrode for the complex 1b, for 2 hours at -2.5 V vs Ag/AgCl.

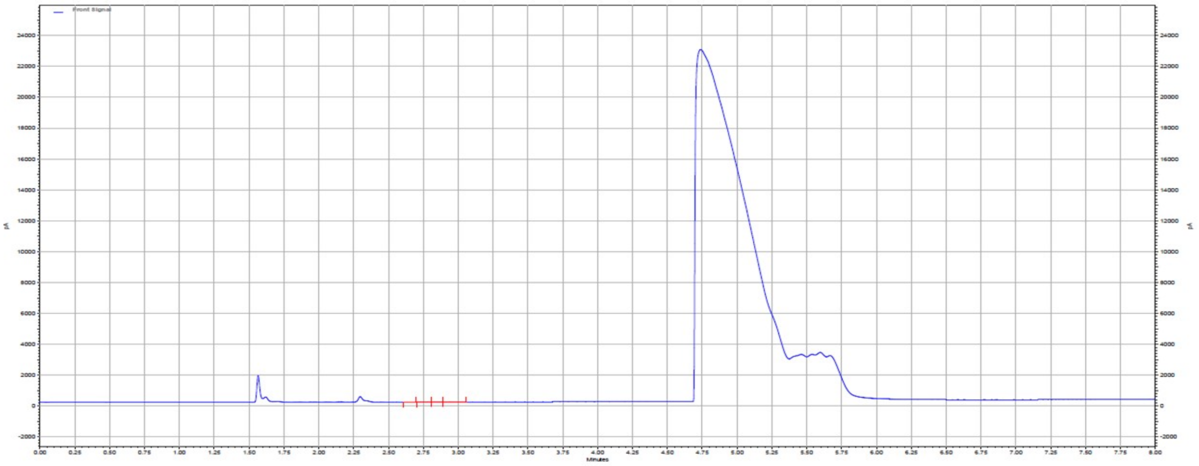

Fig. S36. GC-TCD data after controlled potential electrolyses.

No.	**Solvent(4ml)**	**Electron donor**	**λ (nm)**	**Gas**	**Reduced products**		**TON_{CO}**
					CO (μmol)	**H_2 (μmol)**	
1	DMF/H_2O(4:1)	BIH	$420 \leq \lambda \leq 750$	CO_2	42	0.012	420
2	DMF/TEOA(4:1)	BIH	$420 \leq \lambda \leq 750$	CO_2	26	3.03	260
3	DMA/H_2O(4:1)	BIH	$420 \leq \lambda \leq 750$	CO_2	33	0.01	330
4	DMF/TEA(4:1)	BIH	$420 \leq \lambda \leq 750$	CO_2	5	2.88	50
5	CH_3CN/H_2O(4:1)	BIH	$420 \leq \lambda \leq 750$	CO_2	9	<0.01	90
6	CH_3CN/TEOA(4:1)	BIH	$420 \leq \lambda \leq 750$	CO_2	37	0.01	370
7	CH_3CN/TFE(4:1)	BIH	$420 \leq \lambda \leq 750$	CO_2	22	<0.01	220

8	DMF/TFE(4:1)	BIH	$420 \leq \lambda \leq 750$	CO_2	27	1.32	270
9	CH_3CN/TEOA(4:1)	BIH	Dark	CO_2	0	0	0
10	CH_3CN/TEOA(4:1)	BIH	$420 \leq \lambda \leq 750$	N_2	0	0	0
11	CH_3CN/TEOA(4:1) + 0.1 ml TFE	BIH	$420 \leq \lambda \leq 750$	CO_2	33	0.2	330

Table S10. Photocatalytic CO_2 reduction at different condition. For all catalysts, the photochemical conditions include 4 mL of solvent, 0.2 mM $Ru(dmbpy)_3^{2+}$ as the photosensitizer, 25 mM SED, and 20 µM complex-1a. The quantities of the reduced products generated by the catalysts were measured after 2 hours.

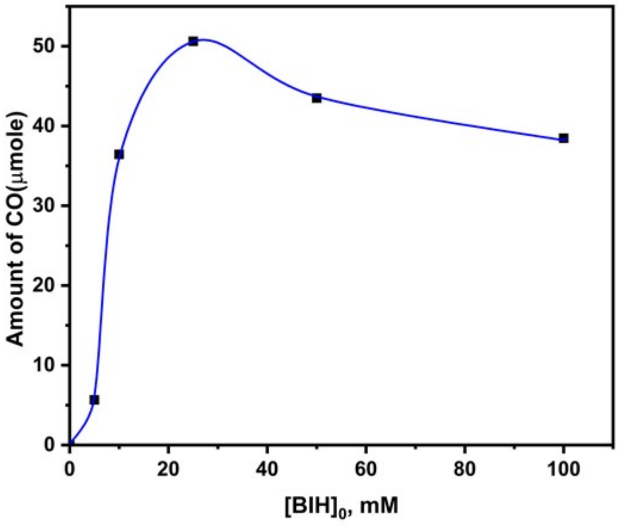

Fig. S37. The amount of CO produced after 4 hours of photocatalytic CO_2 reduction by complex-**1a** as a function of BIH concentration.

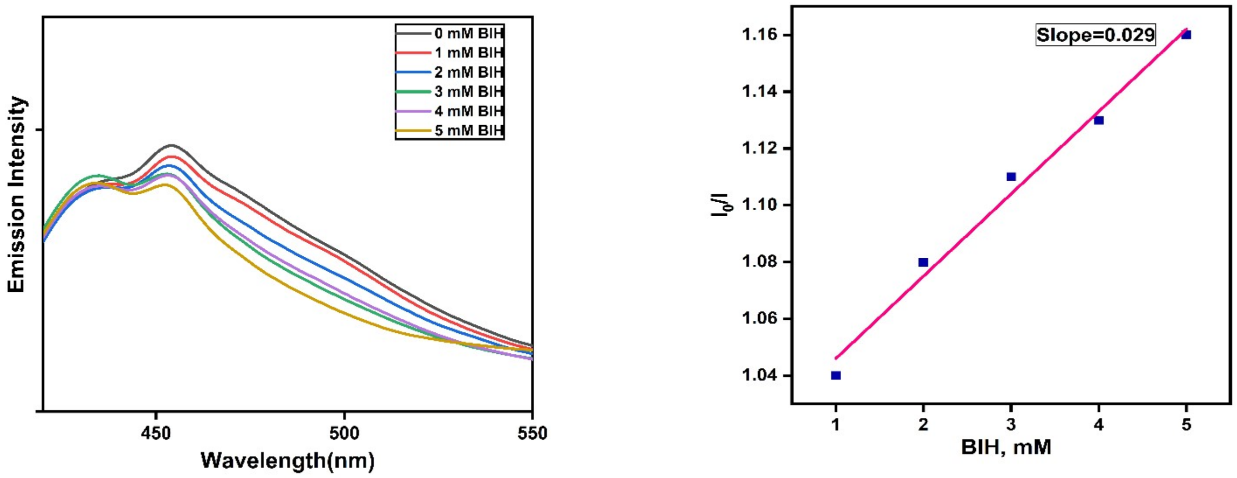

(a) (b)

Fig. S38. (a) Emission spectra of Complex-**1a** (20 µM) excited by monochromatic light at 400 nm CH_3CN containing BIH (0 – 5 mM) at 298 K. (b) A Stern-Volmer plots for the emission quenching by BIH (0 – 5 mM).

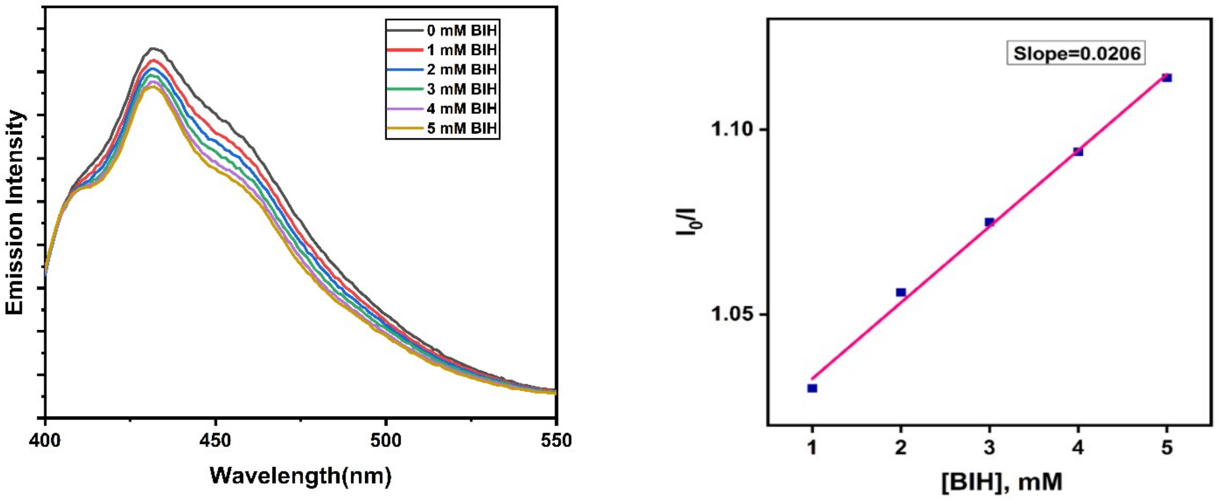

(a) (b)

Fig. S39. (a) Emission spectra of Complex-**1b** (20 µM) excited by monochromatic light at 400 nm CH_3CN containing BIH (0 – 5 mM) at 298 K. (b)A Stern-Volmer plots for the emission quenching by BIH (0 – 5 mM).

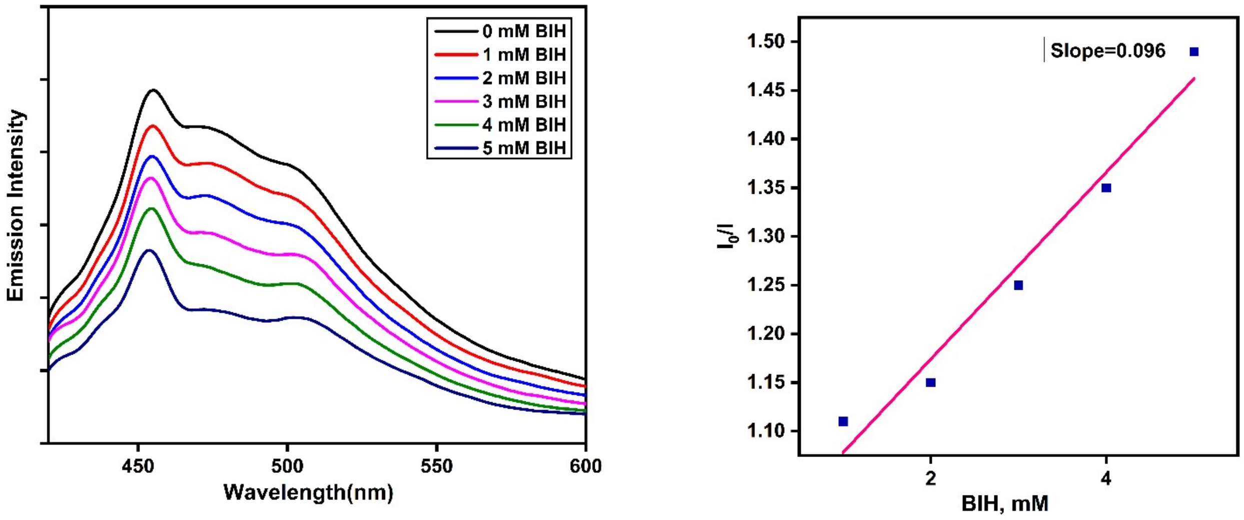

(a) (b)

Fig. S40. (a) Emission spectra of Complex-**1c** (20 μM) excited by monochromatic light at 402 nm CH_3CN containing BIH (0 – 5 mM) at 298 K. (b)A Stern-Volmer plots for the emission quenching by BIH (0 – 5 mM).

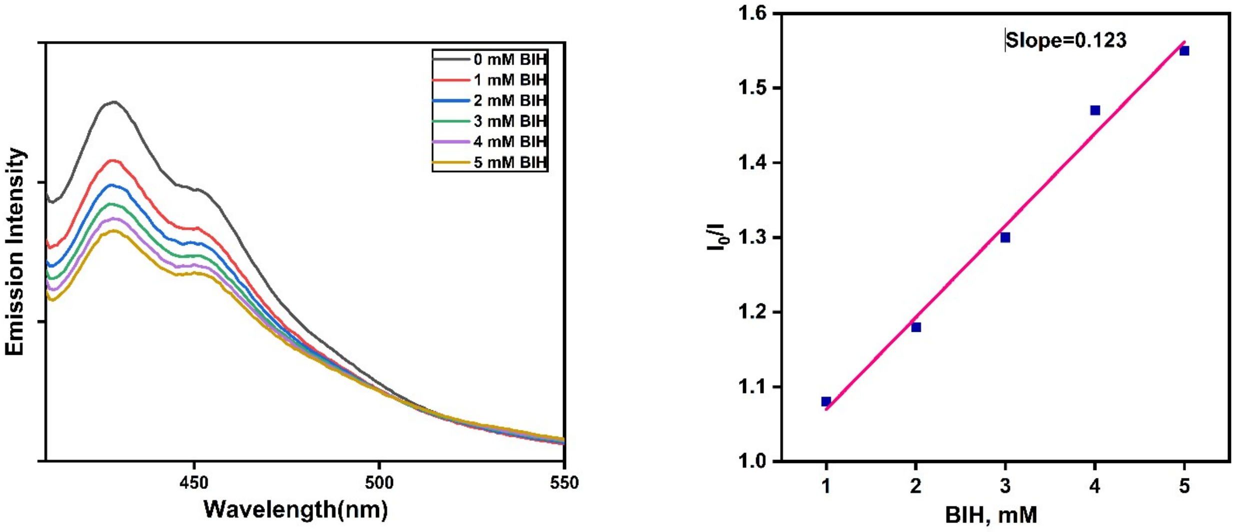

(a) (b)

Fig. S41. (a) Emission spectra of Complex-**2a** (20 µM) excited by monochromatic light at 400 nm CH_3CN containing BIH (0 – 5 mM) at 298 K. (b)A Stern-Volmer plots for the emission quenching by BIH (0 – 5 mM).

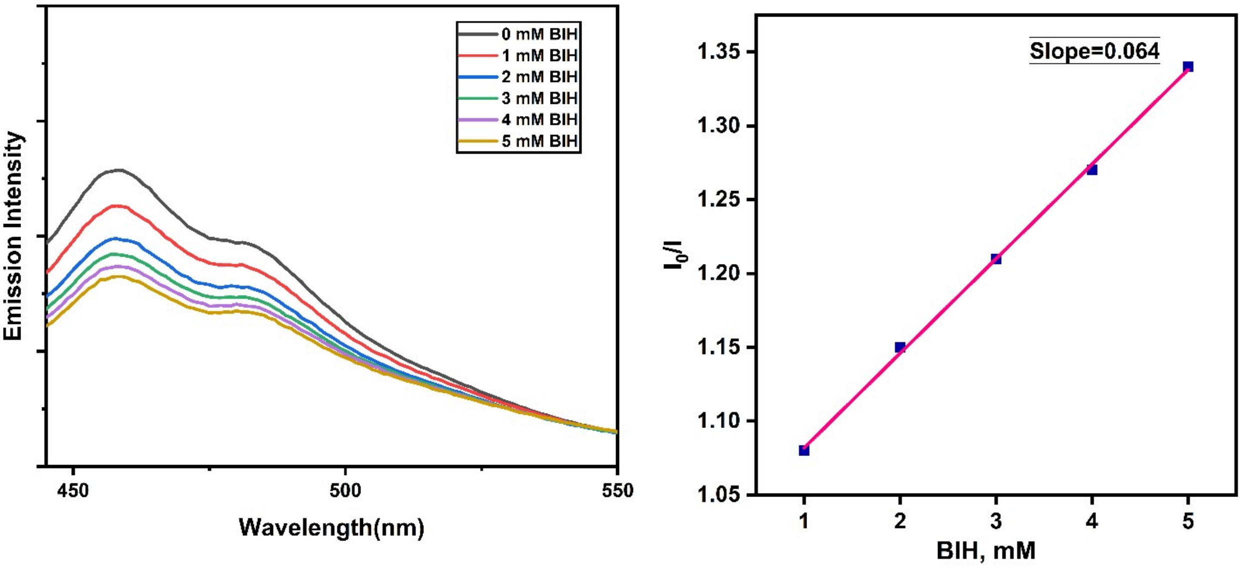

(a) (b)

Fig. S42. (a) Emission spectra of Complex-**2b** (20 µM) excited by monochromatic light at 416 nm CH_3CN containing BIH (0 – 5 mM) at 298 K. (b)A Stern-Volmer plots for the emission quenching by BIH (0 – 5 mM).

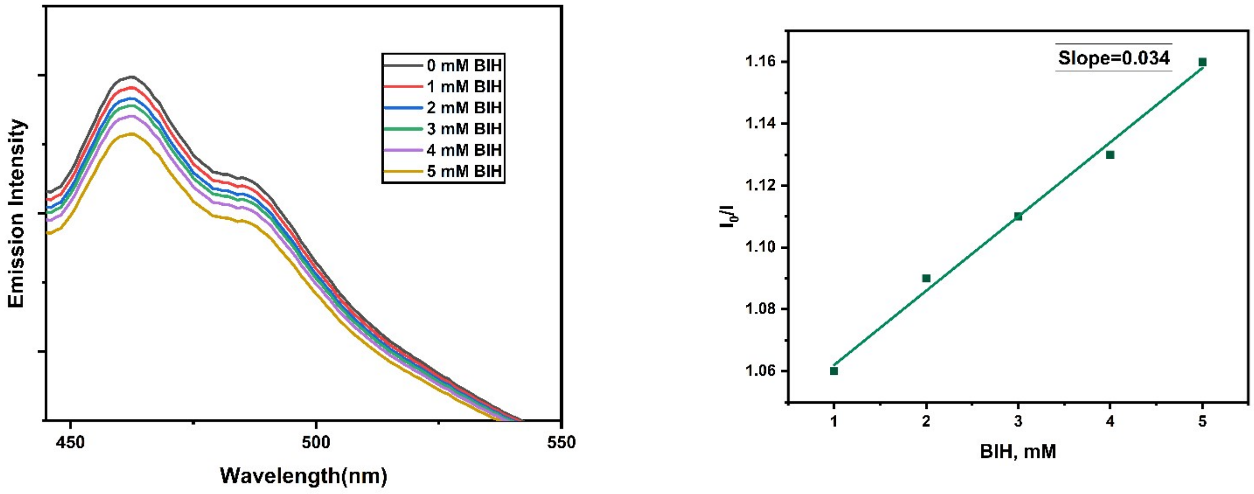

(a) **(b)**

Fig. S43. (a) Emission spectra of Complex-**3a** (20 µM) excited by monochromatic light at 430 nm CH_3CN containing BIH (0 – 5 mM) at 298 K. (b)A Stern-Volmer plots for the emission quenching by BIH (0 – 5 mM).

Catalyst	**K_{SV}(L mol^{-1})**	**k_q (10^9 L mol^{-1} s^{-1})**
1a	**29.0**	**6.9**
1b	**20.6**	**9.7**
1c	**96.0**	**18.2**
2a	**123**	**17.4**
2b	**64**	**31.6**
3a	**34**	**6.4**

Table S11: Stern−Volmer Constants (**K_{SV}**), Reductive Quenching Rate Constants (**kq**) by BIH for the catalysts.

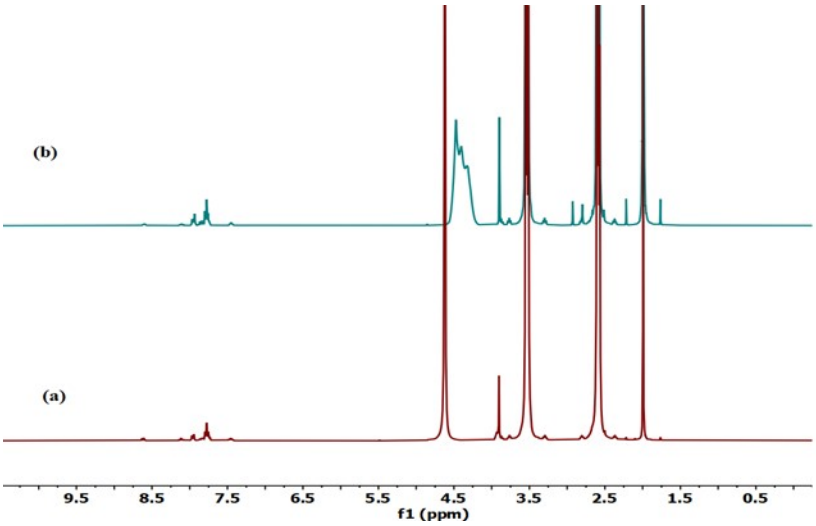

Fig. S44: ^{1}H NMR spectra in CD_3CN/TEOA in the presence of BIH, SP under CO_2 atmosphere and photo irradiation $\lambda \geq 400$ nm , irradiation time 5 hours (a), without catalyst (b) with catalyst

Fig. S45: Photocatalytic reduction of CO_2 in bare sunlight by Complex **1a, 2a and 3a.**

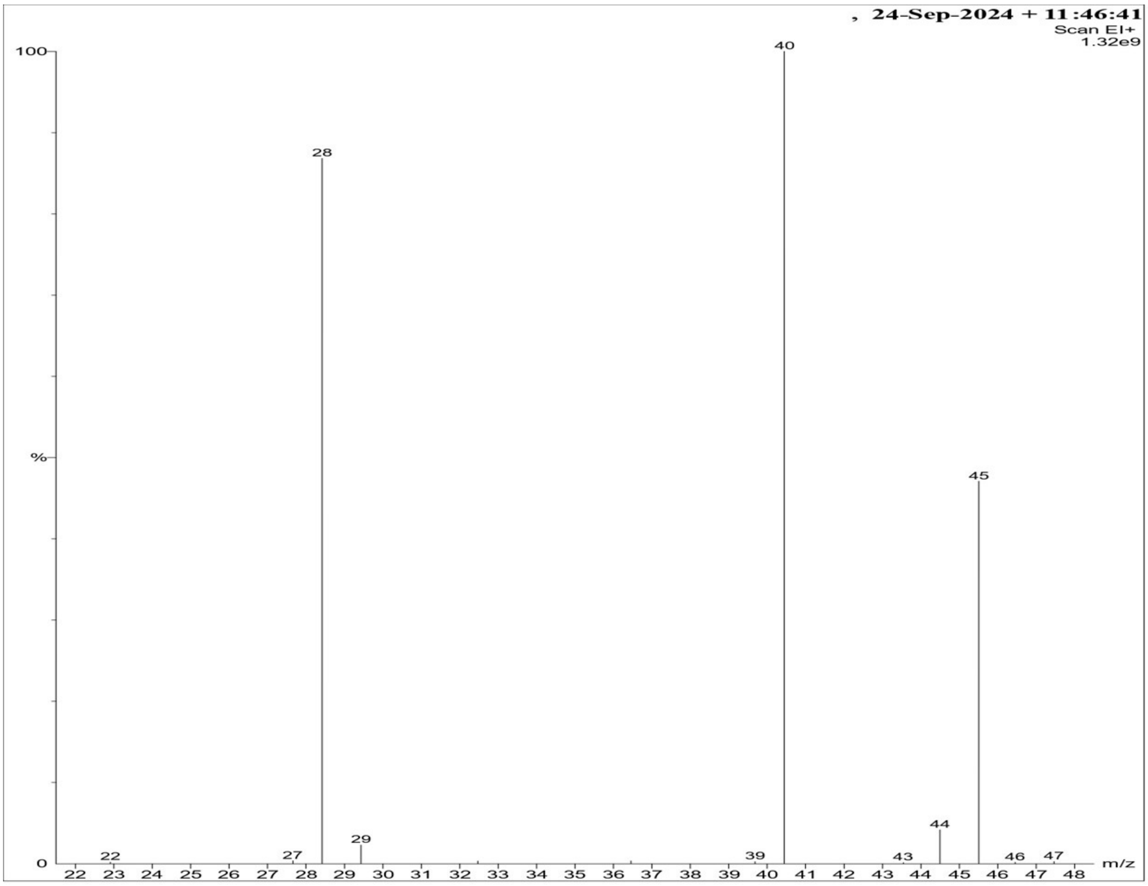

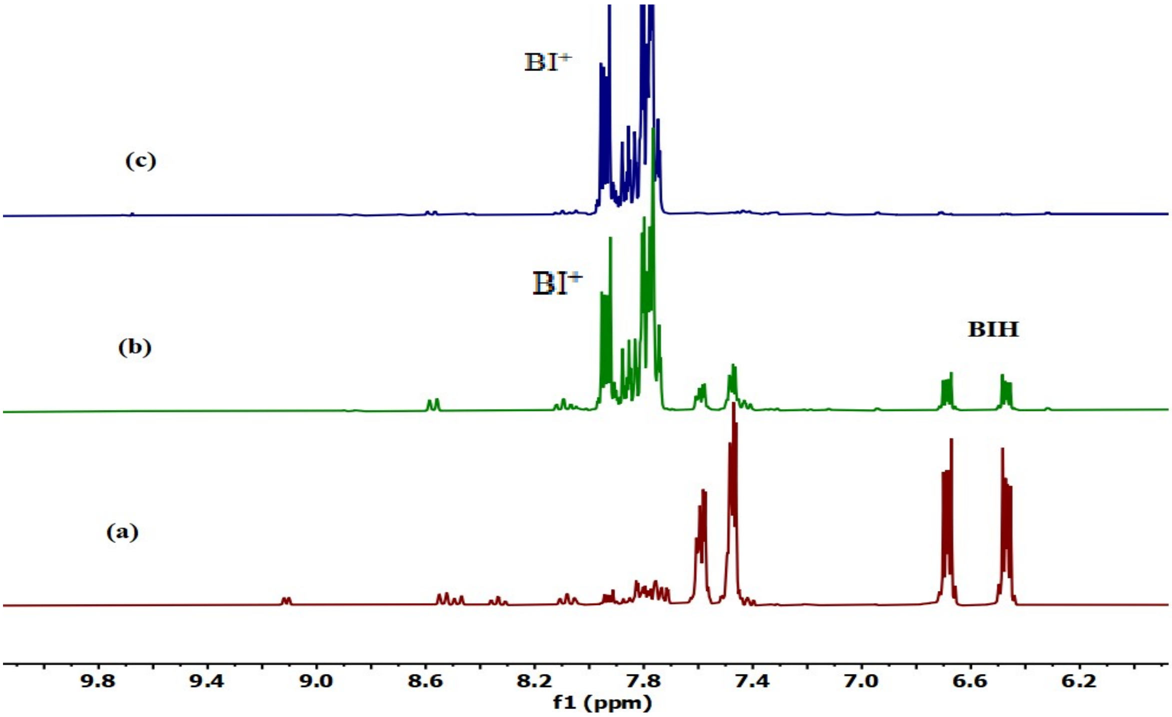

Fig. 46: Mass spectra obtained from GC-MS analysis using labelled $^{13}CO_2$.

Fig. S47: ^1H NMR spectra of **Complex-1b** in CD_3CN/TEOA in the presence of BIH and PS under CO_2 atmosphere and photo irradiation $\lambda \geq 400$ nm , irradiation time 0 min. (a), 60 min (b) 120 min(c)

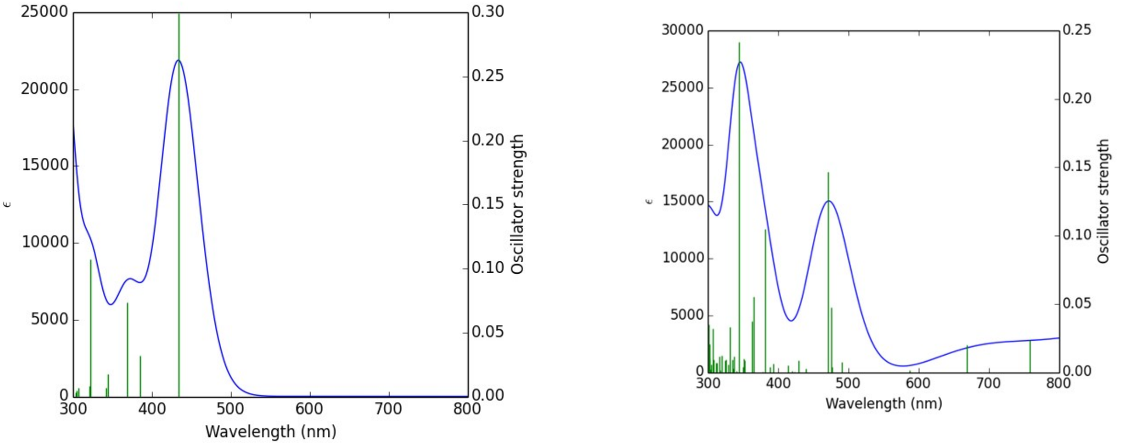

(a) **(b)**

Fig. 48: TD-DFT calculation of **Complex-1b (a)** and its one electron reduced state **(b).**

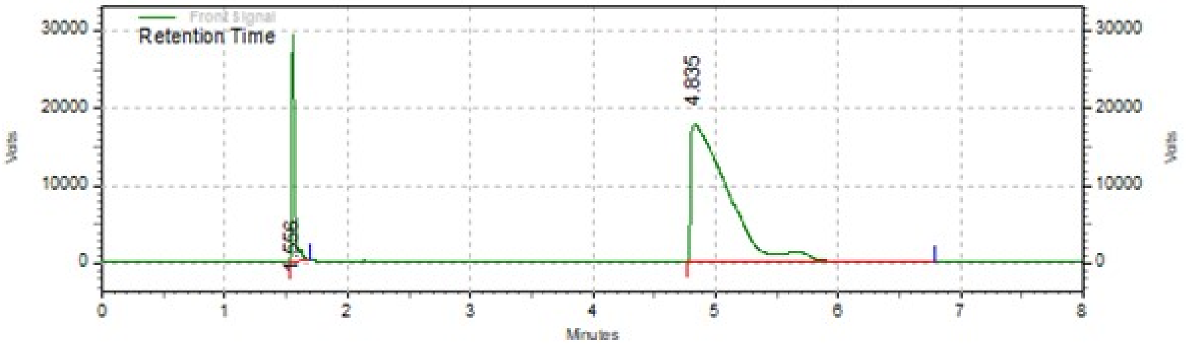

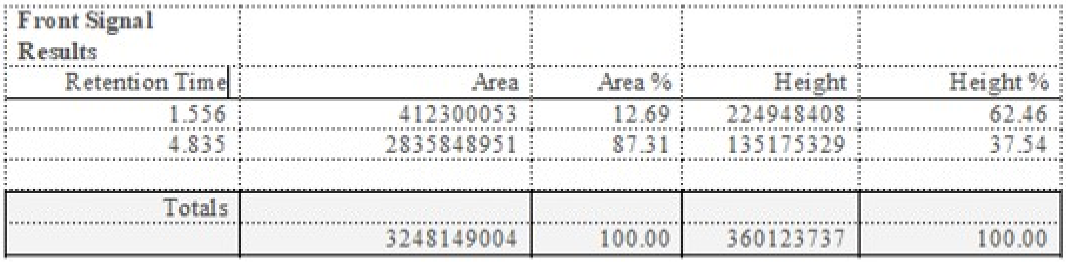

Front Signal Results				
Retention Time	Area	Area %	Height	Height %
1.556	412300053	12.69	224948408	62.46
4.835	2835848951	87.31	135175329	37.54
Totals				
	3248149004	100.00	360123737	100.00

Fig. 49: GC-TCD data for detection and amount calculation for CO.

References:

1. *SMART; SAINT; SADABS; XPREP; SHELXTL,* Bruker AXS Inc., Madison, WI, 1998.

2. G. M. Sheldrick, *SHELXTL, v. 6.14*, Bruker AXS Inc., Madison, WI, 2003.
3. E. Runge and E. K. U. Gross, *Phys. Rev. Lett.*, 1984, **52**, 997 1000.
4. (a) A. D. Becke, *J. Chem. Phys.*, 1993, **98**, 5648–5652; (b) C. Lee, W. Yang and R. G. Parr, *Phys. Rev. B: Condens. Matter*, 1988, **37**, 785–789.
5. (a) M. E. Casida, C. Jamoroski, K. C. Casida and D. R. Salahub, *J. Chem. Phys.*, 1998, **108**, 4439–4449; (b) R. E. Stratmann, G. E. Scuseria and M. J. Frisch, *J. Chem. Phys.*, 1998, **109**, 8218–8224; (c) R. Bauernschmitt and R. Ahlrichs, *Chem. Phys. Lett.*, 1996, **256**, 454–464.
6. (a) V. Barone and M. Cossi, *J. Phys. Chem. A*, 1998, **102**, 1995–2001; (b) M. Cossi and V. Barone, *J. Chem. Phys.*, 2001, **115**, 4708–4717; (c) M. Cossi, N. Rega, G. Scalmani and V. Barone, *J. Comput. Chem.*, 2003, **24**, 669–681.
7. (a) T. Liu, H.-X. Zhang and B.-H. Xia, *J. Phys. Chem. A*, 2007, **111**, 8724–8730; (b) X. Zhou, H.-X. Zhang, Q.-J. Pan, B.-H. Xia and A.-C. Tang, *J. Phys. Chem. A*, 2005, **109**, 8809 8818; (c) X. Zhou, A.-M. Ren and J.-K. Feng, *J. Organomet. Chem.*, 2005, **690**, 338–347; (d) A. Albertino, C. Garino, S. Ghiani, R. Gobetto, C. Nervi, L. Salassa, E. Rosenverg, A. Sharmin, G. Viscardi, R. Buscaino, G. Cross and M. Milanesio, *J. Organomet. Chem.*, 2007, **692**, 1377–1391.
8. (a) P. J. Hay and W. R. Wadt, *J. Chem. Phys.*, 1985, **82**, 270-283; (b) P. J. Hay and W. R. Wadt, *J. Chem. Phys.*, 1985, **82**, 299–310.

9. M. J. Frisch, G. W. Trucks, H. B. Schlegel, G. E. Scuseria, M. A. Robb, J. R. Cheeseman, G. Scalmani, V. Barone, B. Mennucci, G. A. Petersson, H. Nakatsuji, M. Caricato, X. Li, H. P. Hratchian, A. F. Izmaylov, J. Bloino, G. Zheng, J. L. Sonnenberg, M. Hada, M. Ehara, K. Toyota, R. Fukuda, J. Hasegawa, M. Ishida, T. Nakajima, Y. Honda, O. Kitao, H. Nakai, T. Vreven, J. A. Montgomery Jr., J. E. Peralta, F. Ogliaro, M. Bearpark, J. J. Heyd, E. Brothers, K. N. Kudin, V. N. Staroverov, R. Kobayashi, J. Normand, K. Raghavachari, A. Rendell, J. C. Burant, S. S. Iyengar, J. Tomasi, M. Cossi, N. Rega, J. M. Millam, M. Klene, J. E. Knox, J. B. Cross, V. Bakken, C. Adamo, J. Jaramillo, R. Gomperts, R. E. Stratmann, O. Yazyev, A. J. Austin, R. Cammi, C. Pomelli, J. W. Ochterski, R. L. Martin, K. Morokuma, V. G. Zakrzewski, G. A. Voth, P. Salvador, J. J. Dannenberg, S. Dapprich, A. D. Daniels, Ö. Farkas, J. B. Foresman, J. V. Ortiz, J. Cioslowski and D. J. Fox, *GAUS-SIAN 09 (Revision A.1)*, Gaussian, Inc., Wallingford, CT, 2009.